Unified Control Strategy for Microgrid Solid-State Transformers

By Samy Elias

A DISSERTATION SUBMITTED TO

THE FACULTY OF GRADUATE STUDIES

IN PARTIAL FULFILLMENT OF THE REQUIREMENTS

FOR THE DEGREE OF

MASTER OF SCIENCE

GRADUATE PROGRAM IN

ELECTRICAL ENGINEERING AND COMPUTER SCIENCE

YORK UNIVERSITY

TORONTO, ONTARIO September 2022

Abstract

Solid-state transformers (SST) are particularly useful components in distributed generation systems (DG). This research approaches the control of the SST in a more comprehensive and an organized way. It proposes a compact, versatile and an efficient unified control strategy. This proposal gives rise to three more proposals.

i) A method to mitigate the current harmonic distortion which is uniquely software-based and ii) An efficient low-voltage ride-through (LVRT) scheme. Both of those functions come at no extra cost using the proposed unified control scheme. These proposals further demonstrate the proposed strategy's ability to accommodate further features and modifications.

A further contribution to this research addresses the unbalanced load conditions. It proposes a simple, cost-free modification to a resonant filter - making it suitable for the proposed control strategy thus maintaining its simplicity without compromising its practicality.

All the proposals of this research have been validated through simulation in Simulink.

Acknowledgements

I would like to express my gratitude to my supervisor dr. Afshin Rezaei-Zare for his guidance and support not only throughout this research and for his EECS 6706 and EECS 6705 course delivery, but also for his guidance and support during my bachelor's degree, for his undergraduate course delivery, and for the summer research opportunities.

I would like to thank my committee member dr. John Lam for his support and advice as well as for his EECS 6701 course delivery as well as for his undergraduate course delivery.

I would also like to thank my supportive classmates especially Subrina Shawlin and Anusha Lamichhane for their support throughout the past 5 terms.

I am always grateful for the support of my family and friends.

Table of Contents

List of Figures

Nomenclature

SST	Solid-state Transformer
DG	Distributed generation
PV	photovoltaic array
MPPT	maximum power point tracking
HFT	High-frequency transformer
MFT	Medium-frequency transformer
SRC	series resonant converter
PRC	parallel resonant converter
DAB	Dual active Bridge
EMI	electromagnetic interference
Vd	the direct voltage component of the d-q reference frame
Vq	the quadrature voltage component of the d-q reference frame
Id	the direct current component of the d-q reference frame
Iq	the quadrature voltage component of the d-q reference frame
LVRT	Low-voltage ride-through
THD	total harmonic distortion
PI controller	proportional Integrator controller
R-controller	resonant controller
PR controller	proportional resonant controller

Thesis Publications

S. Elias and A. Rezaei-Zare, "Unified Control Strategy for Microgrid Solid-State Transformers," 2022 IEEE International Conference on Environment and Electrical Engineering and 2022 IEEE Industrial and Commercial Power Systems Europe (EEEIC / I&CPS Europe), 2022, pp. 1-6, doi: 10.1109/EEEIC/ICPSEurope54979.2022.9854558.

Chapter 1

Introduction

1.1 Motivation

The Solid-state transformer is a relatively broad research topic – even if only the converters control is considered. Many control schemes have been proposed, whether they were for the isolation stage of the SST or for the inverter – in case of AC connection, in islanded mode or grid-tied mode or the for a smooth transition between the two, or even for controlling the battery energy storage system. However, there does not seem to be work which considers all stages of the SST as a whole - in terms of control - especially in an AC grid where an inverter is needed. This can reduce the efficiency. For example, some proposals concerning Low-voltage ride-through (LVRT) discuss their methods independently of the system – potentially adding extra cost to the system and highlighting the need for a more organized approach. Understanding the interconnectivity and interdependency of the subsystems in relation to one another can lead to better organization and an increase in the possibility of new advancements, as will be shown in this report through a newly proposed harmonic distortion mitigation method which is software based.

The problem can therefore be stated thusly:

SST control lacks organization which reduces its efficiency and raises its cost.

1.2 Organization of the Report

The remainder of this report is organized into the following chapters:

Chapter 2 gives a background to the research by describing and reviewing the SST's physical structure and topologies. It also provides a general background on control and modulation. The relevant literature review is also provided.

Chapter 3 expands the discussion on the control of the SST particularly, the inverter control and the BESS as this will give a more specific background to this research. The relevant literature review is also provided.

Chapter 4 describes the proposed system and proposed the unified control strategy and how the interdependency of all the stages of the SST is considered to achieve better organized and efficient control.

Chapter 5 presents two more proposals. Namely, an efficient LVRT and a software-based harmonic distortion mitigation methods which aim to illustrate the versatility of the proposed control strategy. Literature review pertinent to each of those proposals is also provided.

Chapter 6 presents a resonant controller/filter (R-controller) or (R-Filter) proposal which is implemented in a d-q reference frame rotating at the inverse fundamental frequency after reviewing several approaches and methods of balancing the load voltage in unbalanced load conditions.

Chapter 7 presents seven case studies and their results. The case studies were devised and simulated in Simulink. They validate the proposals described in this report.

Chapter 8 Presents the conclusion of research - highlighting its contributions and their validity. It also provides suggestions for possible future work.

Chapter 2

Solid-State Transformers

2.1 Introduction

Beside the fact the SST is smaller in size compared to the regular transformer, which is achieved through high frequency operation, the use of power electronics in the SST offers various prospects such as better controllability, bidirectionality, and reactive power compensation, and better grid integration. As a result, the SST has become popular in several areas such as renewables and traction systems as well as in power distribution systems. However, the SST introduces various challenges such as the increased cost as well as the reduced efficiency which results from the semiconductors switching and conduction losses in every stage which is then multiplied by the number of stages in the SST. It reduces the power quality as a result of the introduction of harmonic currents back into the grid. Protection issues, and electromagnetic interference (EMI) are also some of the challenges associated with the SST.

Several papers have discussed the SST. [1] and [2] review the SST in terms of its most popular applications, protection challenges and go in good details in its topologies and control. [3] discusses the solid-state transformer in terms of its functions such as voltage transformation, grid integration, etc. and presents possible application areas of solid-state transformer in future smart grids. [4] also discusses potential applications of the SST, and it highlights some challenges related to the cost and efficiency. [5] reviews the main requirements, challenges,

and the state of the art of the SST in traction systems. [6] Highlights the differences between the SST and the regular transformer, pointing out some of the SST challenges such as the cost and efficiency challenges.

2.2 High-Frequency Transformer Considerations

2.2.1 High-Frequency Transformer

Another area of research under SST is the actual high/medium-frequency transformer (HFT/MFT). [2] And [7] Discuss the structure and components of the MFT. [8] discusses the design of medium-frequency transformers for medium-voltage high-power applications. and highlights the trade-offs (efficiency, cost, and power density) as well as its design challenges. [9] proposes an MFT design method, as well as a method to accurately predict the core loss of the MFT. [10] proposes an optimization algorithm for the design of HFT – i.e., the core and the number of turns based of various trade-offs – using multi-physics. A breakdown of the MFT components is provided below.

2.2.2 The Core Geometry

The core geometry is also an important factor in achieving a compact design, sufficient heat dissipation, and the required voltage transfer ratios for an MFT. There are mainly four geometries: core type, shell type, matrix, and coaxial winding transformer (CWT). The main advantage of core type is having two parallel LV windings which result in the reduction of the height of transformer, but it has poor thermal conductivity and so the shell type is better than the core type in that respect. It's mechanical strength along with its better thermal conductivity

makes it less prone to damage by overcurrent. Matrix transformer seems to have both advantages of shell and core types, but it has two main drawbacks which restrict its applications. 1- Using separated core units results in higher volume and weight and consequently increases the total loss and cost. 2- The primary and secondary windings are separated and wound on different legs leading to higher leakage inductance which is not desirable in high power converters. Winding in CWT consists of an outer conducting tube as LV winding. HV winding is thoroughly wound inside this tube. The magnetic cores are around the outer conductor. This topology has low leakage inductance and loss at high frequencies. However, the application of this concept is limited to only high frequency and low power ratings due to the limitation of current carrying capability in the tubular structure. for lower range of frequency and power, the shell type core could be the favorable option, and core type seems to be an appropriate solution for high frequency and power, as concluded by [7].

2.2.3 The Core Material

Another thing to consider when choosing the HFT is the core material. It is typically a soft magnetic material which can be easily magnetized and demagnetized. Four features need to be considered when selecting the magnetic material: (a) low core losses, (b) high saturation flux density, (c) high continuous operating temperatures capability, and (d) high relative permeability. [2] offers a useful comparison between various types of materials based on those criteria.

2.2.4 The Conductors

Because skin and proximity effects are more pronounced at higher frequencies, litz wire or foil conductors are preferred in MFT. Litz wires have low window utilization factor and therefore require larger window area. Reducing the winding losses is obviously desired. One technique which can help to achieve that is interleaving the HV winding with the LV winding. New techniques to that end can be investigated.

2.2.5 Insulation and Thermal Considerations

It is a typical requirement that the insulation should have high thermal conductivity and a high dielectric factor as well as high tolerance to partial discharges. Air is preferred for its cooling effect. Usually, in a highly compact transformers and dry-type transformer, epoxy is used as dielectric material where the high voltage levels prohibit the use of air as a dielectric. For environmental and safety reasons, the use of oil as insulation medium is not preferred. Therefore, using mica tape to insulate the windings, which has high tolerance to partial discharge, is recommended. However, the thermal conductivity of mica is relatively low which can add to the low thermal conductivity of the Litz wire winding if used together. Therefore, other ways to ensure effective heat transfer must be implemented. The insulations of transformers tend to experience a certain amount of stress which is proportional to the magnitude of voltage. Higher switching frequency and higher slew rates in MV voltage level which is typical of SST operation adds a new kind of stress on the SST's insulation system especially with oil-free designs. New dielectric materials and mitigation methods, as well as accurate electric field and dielectric loss calculation techniques, should be

investigated to address this issue. [11] recommends that multi-physics modeling be used to help understand the mechanisms behind pre-breakdown phenomena and as a powerful tool for electrical insulation design.

2.3 The SST Power Electronics

2.3.1 Topologies and Control

2.3.1.1 One-Stage and Two-Stage SST

In the case of one-stage and two-stage SST - (assuming that the DG – for example, a photovoltaic (PV) based system plus its maximum power point tracking (MPPT) - counts as a stage) – the control of the output voltage is done in the isolation stage. Therefore, an appropriate method of control, as well as ways to reduce the conduction and the switching losses need to be implemented. Although some or earlier proposals demonstrated controlling the primary and secondary side SST cell independently without utilizing the MFT's reactive network i.e., using decoupled control, it is more common to have a coupled control. One method of coupled control is to employ a resonance circuit which can temporarily store energy allowing a phase shift between the input voltage and the input current. This has the 2 benefits of reducing the switching loss by causing the current to lag the voltage. Several topologies have been proposed for resonance circuits but can be grouped under the following categories: series resonant converter (SRC), parallel resonant converter (PRC), hybrid series parallel LCC and LLC topology -see fig. 1(a-d). The performance of SRC depends on the accuracy of the resonance frequency of the circuit, which might change as the circuit's passive components age. The Dual active Bridge (DAB) is a non-resonance option to for control - fig. 1-

e. Several techniques have also been used to improve the soft switching operation such as using auxiliary circuits. Other variations on the DAB have also been proposed such as the dynamic current converter (dyna C), and multiple DAB, (MAB). An H-bridge that is controlled at its input side only, is also another option – also fig. 1-e.

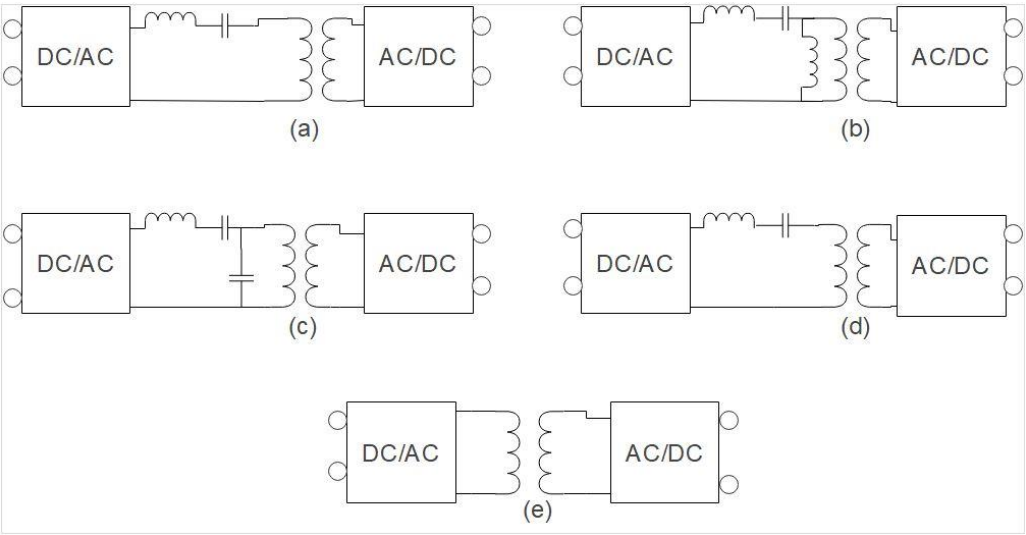

Figure 1. Topologies of single-stage SST - (The isolation stage): (a) Series resonance SST, (b) LLC series-parallel SST, (c) LCC series-parallel SST, and (d) parallel resonance SST, (e) none-resonance SST.

In [12], the isolation stage is designed to achieve soft switching and is implemented using duty cycle modulation. [13] proposes control algorithms to improve the efficiency under light-load conditions in traction systems. [14] proposes control of resonance topology to minimize conduction loss and achieve full-range ZVS to allow for low switching loss and smaller passive components and reduce EMI in a single stage structure. [15] proposes model predictive control (MPC) in a matrix converter-SST connected to ac grids based on the discrete model

of the matrix converter- SST (MC-SST). [16] proposes predictive control in a cascaded modular SST for dc-link regulation and voltage balance. [17] proposes a design to achieve ZVS in an LLC resonance converter. [18] proposes a control method that is duty cycle - phase-shift hybrid to provide wide range of power flow control and voltage regulation.

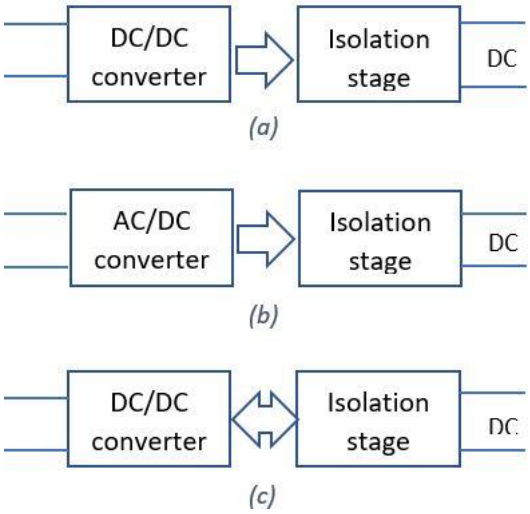

Figure 2. Topologies of two-stage SST: (a) DC/DC SST, (c) AC/DC SST, and (d) Bidirectional DC/DC.

2.3.1.2 Three-Stage SST

In the 3-stage SST, the output voltage control is done in the inverter stage. The Isolation stage of the SST typically operates at resonance frequency with constant 50% duty cycle. The control of the inverter is done using various methods such as a PR controller in the case of [19], or a proportional integral (PI) controller in the case of [20]. A hysteresis current controller is used in [21]. A review to several robust control schemes in different types of microgrids can be found in [22]. A bidirectional SST requires a symmetrical topology for the isolation stage such as

fig. 1- e. It also requires that the output voltage be controlled in the converter stage when it is the output stage. In that case, the inverter is controlled to operate as a rectifier. In the case where the 3-stages SST operates in grid-tied mode as well as islanded mode, the inverter needs to be controlled in both modes, and so a system is put in place to ensure a seamless or a smooth operation when switching between the two modes. Several credible attempts to that end have been proposed by [23], [24], [25], [26], [27], and [28].

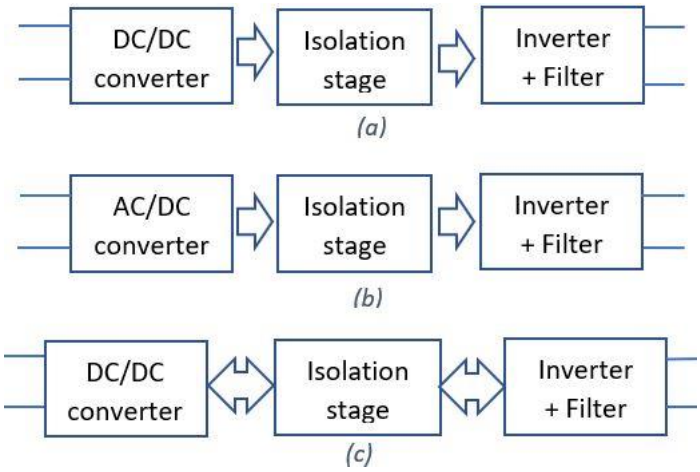

Figure 3. Topologies of three-stage SST: (a) DC/AC SST, (c) AC/AC SST, and (d) Bidirectional DC/AC.

2.3.2 Modulation Schemes

Two level bridge structure is simple to implement but has the has worse harmonic performance compared to multilevel converters. Therefore, multilevel converters with wideband gap semiconductor devices seem to be a better candidate for interfacing MV levels. The most widely used multilevel converters topologies are: (a) Neutral Point Clamped (NPC) or Diode Clamped; (b) Flying Capacitor (FC); (c) Cascaded H-Bridge (CHB); and (d) Modular Multilevel Converter (MMC). Multilevel

switches can increase the levels of EMI. The NPC topology can provide up to five levels but suffers from capacitor voltage balancing issues and higher conduction losses. The FC provides voltage compensation but requires a large amount of storage capacitor, so the system tends to be bulky and expensive. a CHB configuration is modular but have limited performance in terms of reactive power and harmonic compensation in absence of DC voltage supply. MMC is also 3 modular and more robust than CHB as it requires no individual DC voltage supply, but it is more complicated to control, and it has twice the number of switches as CHB. Another comparison between of those schemes can be found in [29].

2.3.3 The Semiconductors

The switches which are used in the inverter and or the isolation stage are mainly either IGBT or MOSFET. The main considerations for the semiconductor switches are 1- the on-resistance which has a direct relation with the conduction loss, 2- the ability for the switch to permit higher frequency operations which will result in lower switching losses, 3- the ability to suit high-voltage and high-current operations, and 4- The cost - as always.

Wide-band-gap semiconductors such as SIC have a band gap that is three times as wide as that of Si and has thermal conductivity that is three times as high as that of Si. The electric field breakdown of SiC is ten times as high as that of Si, allowing for higher operating frequency operations, thereby lower switching losses while significant reducing the size and cost with respect to the power electronics components. Super junction structure that can lead to reduction in the on-resistance compared to the regular SiC-MOSFET is being developed – as discussed in [64] which discusses recent developments SiC devices. [65] discusses medium voltage SiC devices including MOSFETs, IGBTs, GTOs and super-cascode devices.

2.4 Summary

This chapter provided a concise description of the SST and its most prominent aspects namely, its main features, topologies and control, its advantages, and challenges, as well as a review of some of the most interesting research on the SST. The motivation behind this chapter was to give a good yet a concise introduction to the proposals in this report as well as to offer ideas to new researchers as to possible areas of research with respect to SST. Research in terms of semiconductor technologies is left out of this introduction as this should be addressed in semiconductor areas of research rather than power.

Chapter 3

Control Consideration

3.1 Inverter Control

In AC grids, the SST needs to be connected to an inverter which needs to be controlled appropriately for grid-tied operation and/or in islanded mode. To that end, several control methods have been proposed and implemented. [22] reviews several robust control schemes for AC microgrids as well as DC, and hybrid types for different topologies and different ways of connection to power grids. In the case where the DG needs to have the capability to operate in both grid-tied and islanded modes, an appropriate control scheme should be implemented for each mode as well as for the transition from one mode to the other to ensure a smooth transition while considering the complexity of the system, the computational burden, and the overall cost.

[30] and [31] propose a simple algorithm for a seamless transfer between modes of operation. The difference in control in the two modes lies in a current and a voltage controller. The reference to each of the two controllers is changed through the proposed algorithm. The sum output of those controllers is fed into the inductor current controller. So, the system uses three controllers. Both proposals

assume the DG can always provide enough power to match the load voltage to that of the grid, and that is used as a condition before reconnecting to the grid, which can not always be possible. Also, the calculations are not done in the d-q reference frame, which prevents using an integrator in the controller, affecting the steady-state error.

[32] proposes a unified improved droop-based control method, suitable for inverters with LCL filter, through an algorithm that controls and a flag that enables or disables the grid current value fed in the inductor current controller, as well as a switch to connect to the grid after synchronization. The transfer includes an intermediate step which seems to slow the overall response. Also, the paper admits that "reliability in the stand-alone mode needs improvement". [33] offers an automatic change of mode of operation, which is also suitable for inverters with LCL filter. However, the PI voltage controller, which saturates during grid-connected operation, will need to be reset before it can regulate the load voltage in islanded mode. The scheme also requires quite a lot of calculations. [34] proposes a soft start mechanism so as to streamline the switching between PQ control in the grid-tied mode to V/f control in islanded mode and suppress the inrush current when switching to the grid-tied mode. That control method requires a complete control mechanism for each mode which increases the cost. [35] proposes a seamless transfer between the modes of operation, in a droop-based control, by feeding in different references – namely, the output voltage phase reference and the reference to the PI controller. However, different calculations are required to generate the output voltage phase reference which increases the computational burden. The unification in the previously mentioned unified scheme proposals is restricted to controlling the inverter in the two modes of operation.

d-q reference frame current control method is a popular method to control the inductor current. It allows the references and the control variables to be converted to DC quantities. The controller can then be implemented in the same way as DC converters. In the d-q reference frame control, coupling terms between the d and q axis are introduced, and so, they need to be decoupled, as is the case in [36] and [37]. For an L-filter and assuming that the inverter is lossless, (1) and (2) show the coupling of the d and q equations. The first term of the right-hand side is fed forward to decouple the equations – [63]. [38] does away with the decoupling feedforward terms with a proper controller design and the proper choice of the reference current. The input voltage feedforward is added directly to the inverter V_{out} signal. This review is presented in the thesis publication [62].

$$\mathrm{L}\frac{d}{dt}i_d = \omega \mathrm{s}\ \mathrm{iq} + \frac{v_L}{L} \qquad (1)$$

$$\mathrm{L}\frac{d}{dt}i_q = -\omega \mathrm{s}\ \mathrm{id} + \frac{v_L}{L} \qquad (2)$$

Where ω_s is the angular switching frequency, v_L is the inductor voltage, L is the filter inductance and i_d and i_q are the direct and quadrature components of the inverter current respectively.

3.2 BESS Control

Perhaps the most obvious benefit to an energy storage system is that it provides a back up energy in the case of a power outage. However, energy storage systems have been gaining popularity for different reasons. A micro-grid, also known as a distributed generator (DG), especially one that is based on a solar or wind power sources, requires an energy storage system to help mitigate the large fluctuation in energy production which is typical of those power sources. To that end, [39] proposes a method for sizing the battery. It highlights the sizing method, cost, the

estimation of the life span of the system, as well as the peak shaving function. However, this paper does not offer a control algorithm. [40] seeks to help regulate the load frequency in islanded mode through a control scheme based on the shift droop method as a way of regulating the load frequency. The SoC was better controlled and therefore the availability of the BESS was improved when compared to the LFC method or the conventional droop method. Another important function of BESS is to achieve peak-shaving. [41] proposes a control scheme which successfully achieves peak-shaving of the feed-in PV power. while optimizing the capacity of the battery by employing a feedback-adjustment scheme. [42] uses the predictability of a particular institution to propose a suitable control scheme to efficiently achieve peak-shaving. The control scheme can only be replicated in complexes with predictive consumption pattern and few number of peaks. [43] proposes a method to dynamically calculates the demand to better control the BESS for various possible cases of demand and PV profiles to optimize peak shaving.

3.3 Summary

This chapter provided a paper review of some of the inverter proposed techniques especially ones which discuss a seamless transition between the two modes of operation, i.e., islanded and grid-tied modes. This chapter also provides a paper review of BESS control schemes to achieve efficient peak-shaving. Not only is the paper review relevant to the proposals in this report, but it also highlights the observation made in the motivation section that research on SST control tend to focus on one particular stage without considering all the stages as a whole.

Chapter 4

The Unified Control Strategy

4.1 Introduction

The isolation stage of SST in discussion is connected to a PV array through a boost converter with MPPT capability. At that DC link, the battery is connected through a buck-boost converter. The isolation stage is a bidirectional H-bridge. The other side of the H-bridge – let's call that the output side – is connected to a three-phase two-level inverter which is connected to the AC grid and a parallel critical load. Fig. 4 and Fig. 5 illustrate the layout of the system and the SST respectively.

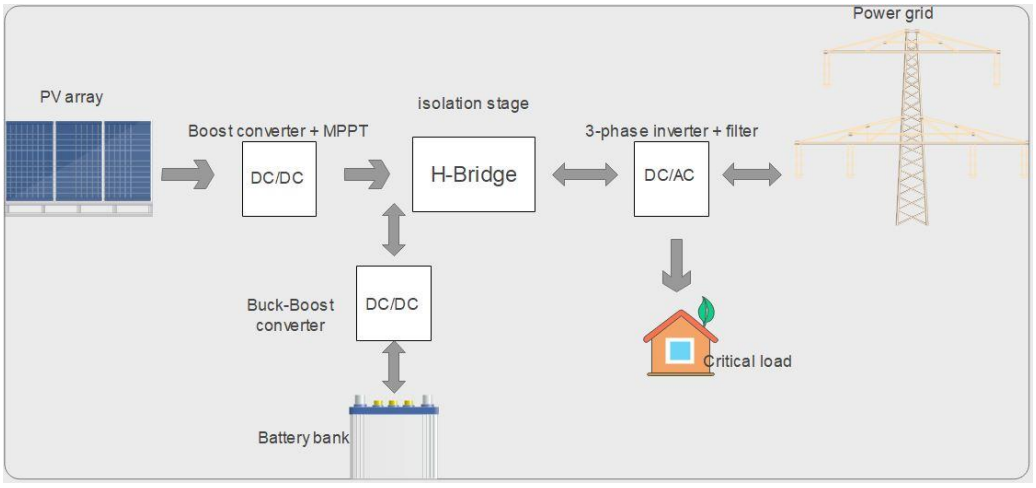

Figure 4. The layout of the system

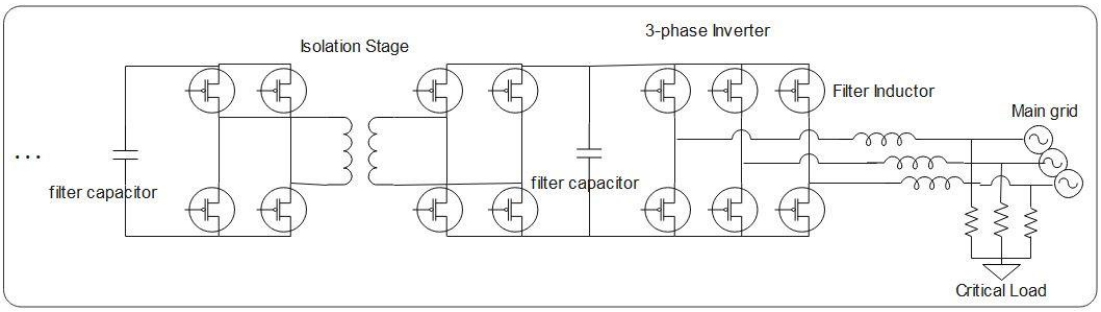

Figure 5. The SST topology

4.2 Inverter Control in the Proposed System

An inverter control scheme for islanded mode and another for grid-tied mode are carefully chosen so that they can both be combined in one system thus doing away with the redundant components and cutting the hardware components count almost by half. This also makes a smooth transition between the two modes much easier. Fig. 6 depicts those two control schemes.

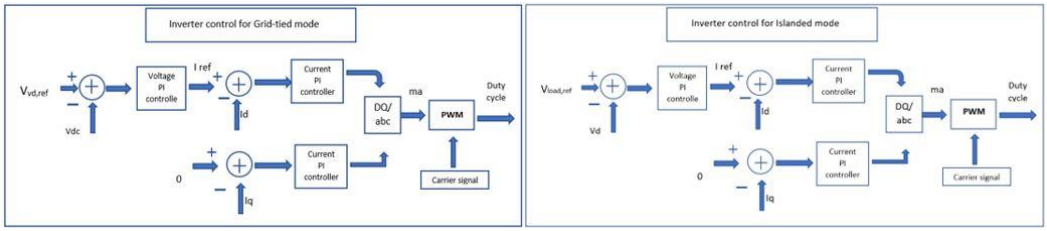

figure 6. Inverter control schemes. Left: gid-tied mode control scheme - Right: Islanded mode control scheme

The control is performed in the synchronous (dq0) reference frame. The dq0 transformation is given by:

$$X_{dq0} = T_\theta \ . \ X_{abc} \quad (3)$$

$$X_{abc} = T_\theta{}^{-1} \ . \ X_{dq0} \quad (4)$$

Where,

$$T_\theta = \frac{2}{3}\begin{bmatrix} \cos(\theta) & \cos\left(\theta - \frac{2\pi}{3}\right) & \cos\left(\theta + \frac{2\pi}{3}\right) \\ -\sin(\theta) & -\sin\left(\theta - \frac{2\pi}{3}\right) & -\sin\left(\theta + \frac{2\pi}{3}\right) \\ \frac{1}{2} & \frac{1}{2} & \frac{1}{2} \end{bmatrix} \quad (5)$$

And,

$$T_\theta{}^{-1} = \begin{bmatrix} \cos(\theta) & -\sin(\theta) & 1 \\ \sin\left(\theta - \frac{2\pi}{3}\right) & -\sin\left(\theta - \frac{2\pi}{3}\right) & 1 \\ \cos\left(\theta + \frac{2\pi}{3}\right) & -\sin\left(\theta + \frac{2\pi}{3}\right) & 1 \end{bmatrix} \quad (6)$$

And θ = ωt – [63]

In the grid-tied mode omega is the angular frequency of the grid. In the islanded mode, ωt is generated independantly at a constant value which is the ideal grid frequency. i.e., 2π60.

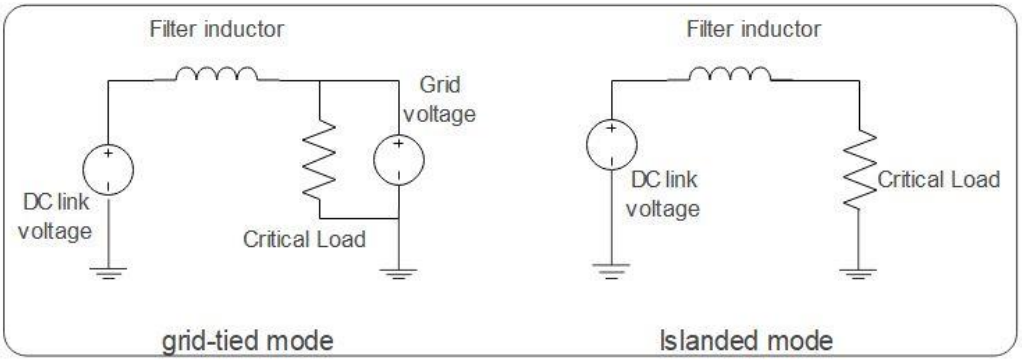

Figure 7. The inverter equivalent circuit in the grid-tied mode (left) and the islanded mode (right)

The equivalent circuit in the grid-tied mode (Fig.7, Left) includes two voltage sources and can therefore be solved with the superposition principle. In one circuit, with only the DC link voltage (Vi) as a voltage source, the impedance of the grid is much smaller than that of the parallel load, and so the inductor current will depend on the filter inductance and Vi. In the second circuit, with the grid voltage

is the only voltage source, the inductor current will depend on the grid voltage and the current division between load impedance and the filter inductor.

In the Islanded mode (Fig.7, Right), the inductor current will depend on Vi and the series impedance of filter inductive reactance and load impedance.

The inductance of the filter is given by (7).

$$L = \frac{UV_L}{\omega \frac{P}{3}} \quad (7)$$

Where, U is the output voltage. V_L is the inductor voltage which is typically around one tenth of the output voltage. ω is the angular frequency of the output voltage. P is rated power.

When the grid current drops to close to zero, indicating the disconnection of the grid – note that what triggers the disconnection of the grid is not discussed in this paper - an if statement in the function specifies the reference to the voltage loop, as well as specifying the load voltage as feedback voltage which is then subtracted from the given reference to generate the error signal. The values of Kp and Ki of the voltage and current controllers are changed appropriately. The reference voltage is chosen to match the grid voltage. When the grid current rises above the chosen threshold value (almost zero), the reference to the voltage loop is changed to a predetermined value which is chosen to be slightly higher than the sum of the grid voltage and the inductor voltage to guarantee power transfer. The DC link voltage is inputted as the feedback voltage to be subtracted from that reference value and generate the error signal. The Kp and Ki values of the voltage and current PI controllers can be changed appropriately.

The reference current to the inductor current controller in the grid-tied mode is generated from the difference between the input DC voltage to the inverter (Vi) and an appropriately chosen reference voltage. As the power varies, (Vi) is regulated by varying the inverter current through varying the reference current.

In the islanded mode, the reference current is generated through regulating the load voltage.

A MATLAB function is used to compensate for the differences in the original control schemes or the two modes by outputting the appropriate control variables for the desired mode of operation as shown in fig. 8. This analysis is also provided in the thesis publication [62].

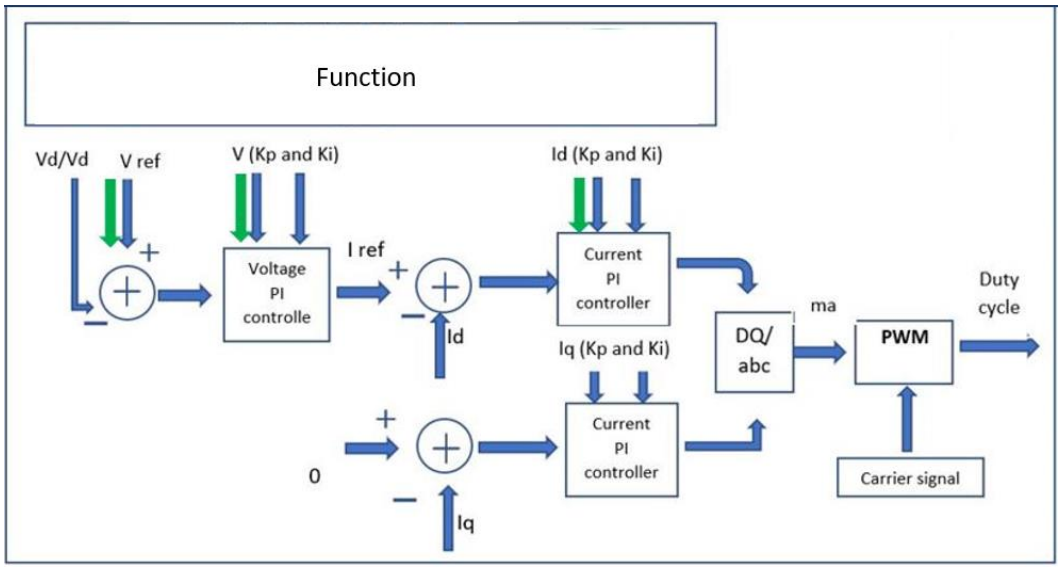

Figure 8. The unified inverter control

4.3 BESS Role in the Proposed System

The control scheme for the battery energy storage system (BESS) is incorporated into that MATLAB function. The function outputs the reference current for the battery to the battery PI controller. The battery needs to inject the appropriate amount of power to aid with the load voltage regulation in islanded model. The BESS ends up performing several functions in the bigger scheme. Besides the load voltage regulation, the BESS is utilized to achieve peak-shaving. It helps absorb the

excess energy in the LVRT scheme. And it takes the harmonics distortion into account in its operation – as will be further discussed. This highlights how the proposed unified control scheme considers the interconnectivity of the different stages of the SST to achieve a more organized and therefore a more efficient system. Fig. 9 illustrates the flow chart of the main algorithm.

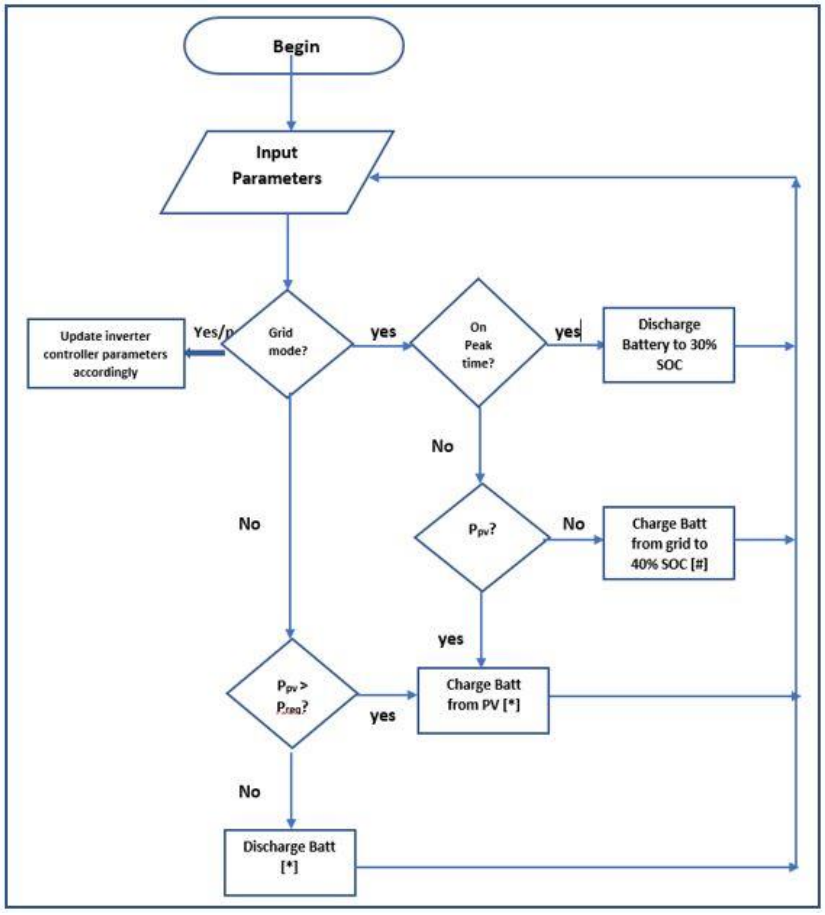

Figure 9. The main unified control algorithm

4.4 H-Bridge Control

Since the SST in this system is bidirectional, both sides of the H-Bridge are controllable semiconductor switches rather than having diodes in the output side.

The H-Bridge is not needed for voltage regulation, and so it works at a constant 50% duty cycle. The output-side switches are turned off. The H-bridge is connected to the PV through a boost converter with MPPT capability.

The battery needs to have some power available for use in an emergency power outage and so, if there's not enough solar power to recharge it to a safe level, the algorithm will reverse the direction of power through the control of the H-bridge so that the battery can be charged from the grid. The H-bridge will continue to work the same. That is to say, the output-side switches will be turned off, and the input-side ones will operate at a constant and complementary 50% duty cycle, only the input and output sides are reversed. The control scheme for the SST H-bridge is included in the main function so that bidirectionality can be coordinated with the BESS control.

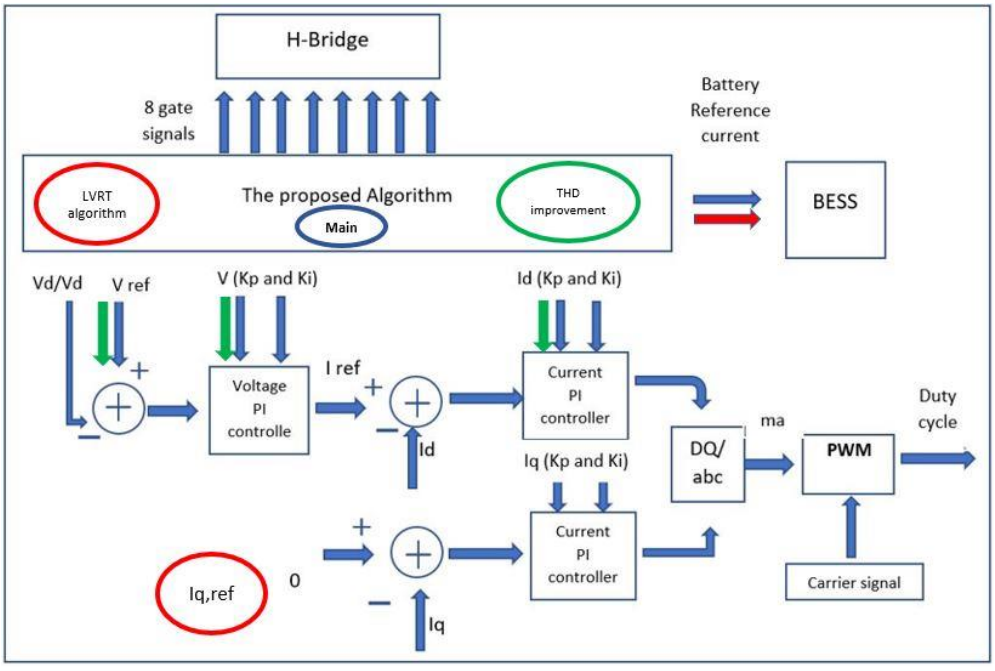

Figure 10. The main unified control scheme

4.5 Summary

This chapter discussed the methodology of the unified control scheme which uses two similar control schemes one for each mode of operation and combining them in one, doing away with the redundant components. The two schemes are unified with the help of a function which will prove even more useful than for just that. The smooth transfer between the two modes is simplified. The control scheme also includes the control of the isolation stage – as well as the BESS control which were also described.

Now that the control of all stages of the SST is in one place - in the same function, any extra method can be added cost-free since a good infrastructure has been established. here, two extra methods are proposed and added. The first one is an efficient LVRT method, and the second method is a new harmonic distortion mitigation method that's purely software implemented. The final control scheme is shown in fig. 10.

Chapter 5

Additional Proposed Methods

5.1 Introduction

So far, a unified control scheme has been presented. The scheme is designed to be comprehensive yet compact so as to offer a good and a convenient infra-structure which can accommodate new functions or future modifications. To illustrate this point, two functions are also proposed in this research in addition to the main unified control scheme proposal. 1) a harmonic mitigation method that's software implemented. 2) an efficient low-voltage ride-through (LVRT) scheme. Both come at no extra cost - in terms of hardware.

5.2 LVRT

5.2.1 Introduction

Grid codes require the DGs to have low voltage ride-through (LVRT) capability. This entails limiting the current that is injected to the grid to the rated current as well as injecting reactive power into the grid in order to help stabilize the grid voltage and frequency. Several schemes and algorithms have been proposed on the subject of LVRT.

[44] proposes a modification to the regular PO method for MPPT to help achieve the power required for LVRT by setting a reference and controls the voltage based on whether the difference between the actual power measurement and the power reference is increasing or decreasing. [45] to allow for reduction of solar power and regulation of the DC link. The paper provides detailed calculations of the active and reactive current required during the LVRT operation.

[46] improves the efficiency of the algorithm by letting only a small part of the it to run continuously. The algorithm also reduces the calculations by incorporating a delay once a voltage sag is detected and required current reference values have been calculated. The paper does not provide a detailed explanation of the actual LVRT control.

[47] incorporates a BESS system to help with the energy management during LVRT operation. It also proposes recurrent wavelet petri fuzzy neural network (RWPFNN) controller to provide a faster response to voltage sags which is the focus of that paper. [48] proposes a supercapacitor (SC) energy storage system (SCESS) to absorb the excess solar power during voltage sags. The paper does not present a comprehensive scheme as to how to generate the DC link voltage reference or whether a voltage sag is the only scenario in which the SC can charge.

5.2.2 The Proposed LVRT

In this method, the BESS allows the MPPT to work through the fault - avoiding unwanted transient effects - unlike some other LVRT proposals.

The algorithm uses a minimal number of calculations, and it does not run any unnecessary calculations as is the case with some other reviewed work.

The LVRT method is implemented in the main function. The function outputs Iq reference to inject reactive power in the grid to help stabilize it as per the

requirements. It also uses the BESS to absorb the extra energy thereby keeping the inverter current at maximum of its rated value. The BESS already exists in the system, so the LVRT functionality comes at no extra cost to the system.

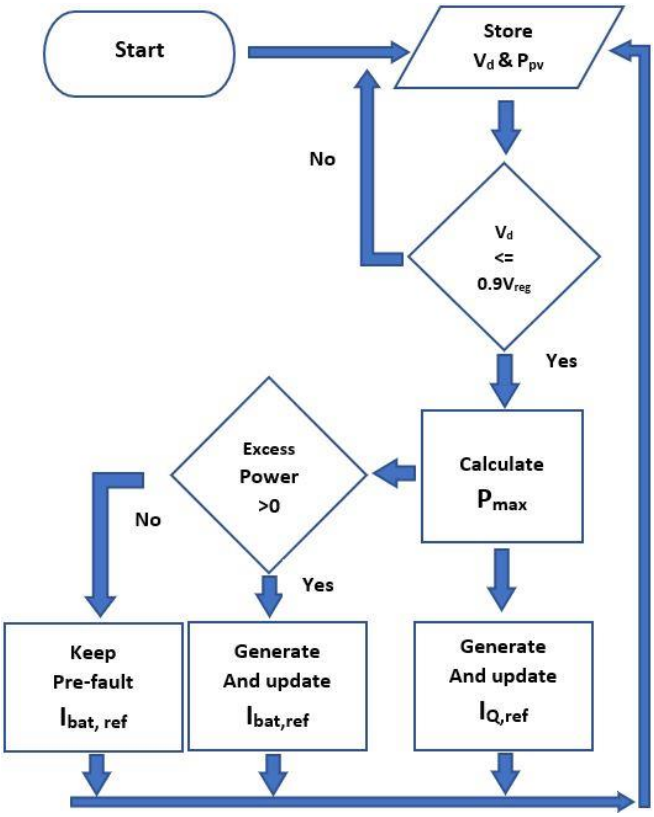

figure 11. The LVRT algorithm.

5.3 Harmonic Distortion Mitigation

5.3.1 Introduction

The three-phase bridge of the inverter produces six pulses per cycle on the output. It produces triple-N harmonics as well as the fifth and seventh harmonic. Conventional methods to reduce harmonics include i) delta-wye isolation

transformer which traps the triple-N harmonics in the delta, ii) passive filters which can be tuned to a single harmonic or a band of harmonics, and iii) active filters which updates the tuning of the conditioner to avoid it falling out of tune in case of harmonic shift - [49].

5.3.2 The Proposed Harmonic Distortion Mitigation Method

The conventional methods for harmonic distortion mitigation discussed above require bulky and costly components unlike the method proposed in this report which is software based and involves a minimal number of calculations, given the pre-existing infrastructure given by the unified control scheme. This method is described as follows:

In the grid-tied mode, the reference voltage to the inverter is usually chosen to be slightly higher than the grid voltage plus the voltage across the filter.

Since the filter voltage drops as the current injection drops, we can use a lower reference voltage without running the risk of saturating the controller, thus increasing the current and reducing the harmonic distortion. When the current is very low and therefore has high THD, we should increase the reference voltage to suppress the current even further eliminating most of that harmonic distortion that is characteristic of low current. The reference voltage is updated in the main function along with some control parameters and so, the proposed THD improvement method is implemented with a few lines of code without any extra components. It should be noted that the battery should only be allowed to charge from the PV at power levels that are high enough to avoid high harmonic distortions, which also is facilitated by the unified control algorithm.

This is a new Harmonic Distortion improvement method which is only possible because of the good infrastructure that the proposed unified scheme offers.

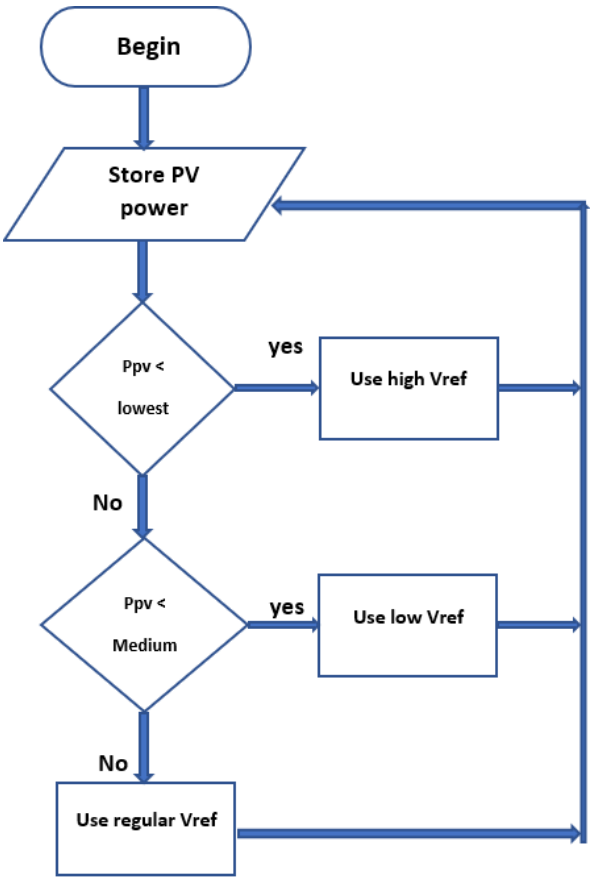

figure 12. The harmonic distortion mitigation algorithm.

The flow chart depicted in Fig. 12 illustrates and highlights the simplicity of the implementation of the new harmonic distortion mitigation method within the main function having established the main unified control scheme.

5.4 Summary

This chapter introduced further contributions to the main proposal. Namely an LVRT which was shown to be efficient for several reasons, and a new harmonic distortion method that is software implemented which means it comes at no cost to the system given the solid infrastructure established by the main unified control scheme. The introduction of those two methods illustrates the opportunity for tackling various challenges cheaply and more efficiently through the same way. That's to say, through establishing a similarly organized infrastructure for a given system.

Chapter 6

Voltage Regulation in Unbalanced Load Conditions

6.1 Introduction

So far, an organized and an efficient system has been established. However, the inverter control schemes which were used as a starting point have their limitations in terms of load voltage regulation in unbalanced load conditions, yet those systems were chosen for their simplicity - as simplicity was one of the objectives of this research.

To add that functionality to the proposed unified control strategy, two possible options were available to explore:

a- To start over with control scheme that is more suitable for unbalanced load conditions:

Inverter control schemes which have that functionality tend to have an LCL, unlike the one subject to this research which has an inductor filter, as seen fig. 5 and fig. 7. [50] is one such example. Its proposed scheme does not need to switch between the two modes. The voltage controller is allowed to saturate in the grid-tied mode

and the inverter is controlled as a current source. However, besides the fact that the system might respond slowly as the voltage controller recovers from saturation to work in the islanded mode, the LCL filter is bigger and more expensive, and the scheme is complicated and uses more sensors and mathematical calculations. [51] proposes another control scheme which effectively regulates the voltage in unbalanced load condition. It separates the positive sequence and the negative sequence. The sequences are then controlled in two different loops. The positive and negative sequence are otherwise coupled. It too employs an LCL filter. Another disadvantage, besides those of the LCL filter, is having to double the number of control loops. [52] offers a similar proposal, but it is in the stationary reference frame rather than the synchronous reference frame as the previously mentioned papers. It uses a virtual resistor based active damping methodology based on indirect capacitor current feedback to cancel out the resonance oscillations due to the third order (LCL) filter which highlights another disadvantage of the LCL filter.

Although it would be a good opportunity to test the adaptability of the proposed unified control strategy by testing it with different control schemes, as discussed, those schemes have their disadvantages which need to be addressed.

b- To modify the system so as it can regulate the load voltage in islanded mode unbalanced load conditions:

Resonant controllers and digital filters are used for reducing the steady state error as well as for harmonic compensation. The PR control theory explained in [53]. [54] Discusses the design procedure for the resonant controller. Load imbalance creates negative second harmonic in the d-q reference frame. The R-controller should be tuned to the second harmonic to compensated for the voltage imbalance – Ref [55]. The proportional resonant (PR) controller has the advantage

of compensating in the positive and negative sequence simultaneously – [54]. [56] proposes a multi-resonant controller to compensate for the 2nd harmonic caused by the unbalanced load condition as well as two more compensators for the harmonics caused by non-linear loads. It is possible, or even probable, that the compensation for non-linear load harmonics obscured the fact that the first compensator produces the inverse 5th and the direct 7th harmonics. [57], [58], and [51] propose decoupled sequence control. That is to decouple the negative and positive sequence and control them separately. The coupling relation is given by (8) through (13) - The obvious disadvantage is, of course, having to double the number of controllers.

$$Vdq^n = \begin{bmatrix} Vd^n \\ Vq^n \end{bmatrix} = \begin{bmatrix} \bar{V}d^n \\ \bar{V}q^n \end{bmatrix} + \begin{bmatrix} \tilde{V}d^n \\ \tilde{V}d^n \end{bmatrix} \tag{8}$$

$$\begin{bmatrix} \bar{V}d^n \\ \bar{V}q^n \end{bmatrix} = V^n \begin{bmatrix} \cos(\varphi^n) \\ \sin(\varphi^n) \end{bmatrix} \tag{9}$$

$$\begin{bmatrix} \tilde{V}d^n \\ \tilde{V}q^n \end{bmatrix} = V^m \cos(\varphi^m) \begin{bmatrix} \cos((n-m)\omega t) \\ -\sin((n-m)\omega t) \end{bmatrix} + V^m \sin(\varphi^m) \begin{bmatrix} \sin((n-m)\omega t) \\ \cos((n-m)\omega t) \end{bmatrix} \tag{10}$$

and

$$Vdq^m = \begin{bmatrix} Vd^m \\ Vq^m \end{bmatrix} = \begin{bmatrix} \bar{V}d^m \\ \bar{V}q^m \end{bmatrix} + \begin{bmatrix} \tilde{V}d^m \\ \tilde{V}d^m \end{bmatrix} \tag{11}$$

$$\begin{bmatrix} \tilde{V}d^m \\ \tilde{V}d^m \end{bmatrix} = V^m \begin{bmatrix} \cos(\varphi^m) \\ \sin(\varphi^m) \end{bmatrix} \tag{12}$$

$$\begin{bmatrix} \tilde{V}d^m \\ \tilde{V}q^m \end{bmatrix} = V^n \cos(\varphi^n) \begin{bmatrix} \cos((n-m)\omega t) \\ \sin((n-m)\omega t) \end{bmatrix} + V^m \sin(\varphi^n) \begin{bmatrix} -\sin((n-m)\omega t) \\ \cos((n-m)\omega t) \end{bmatrix} \tag{13}$$

Where Vdq^n and Vdq^m are two reference frames rotating at nω and mω respectively, and n and m can be either positive or negative. The bar accent denotes DC, and the Tilda accent denotes AC.

6.2 New Proposal for a Resonant Filter

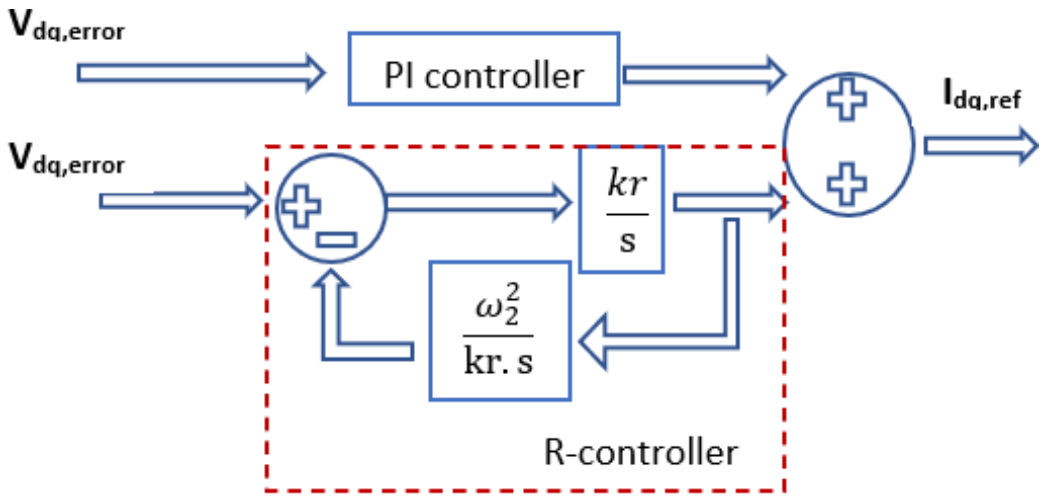

figure 13. The Resonant controller

This research also proposes a Resonant controller - Fig. 13 – to be used with the PI controller to balance the load voltage in the islanded mode. The R-controller/filter is tuned to the second harmonic. The transfer function of the R-controller is given by (14), the transfer function of the PI controller given by (15), and the overall transfer function for the voltage controller is given by (16). The synchronous reference frame rotates at the inverse fundamental frequency. This help to avoid the added harmonics which are seen when the d-q reference frame rotates at the direct fundamental for the same R-controller setup, namely the

inverse 5^{th} and the direct 7^{th} harmonics - see case study 6. As mentioned earlier in chapter 4, ωt is generated independantly at a constant value which is the ideal grid frequency. i.e., 2π60 as can be be seen in fig. 14.

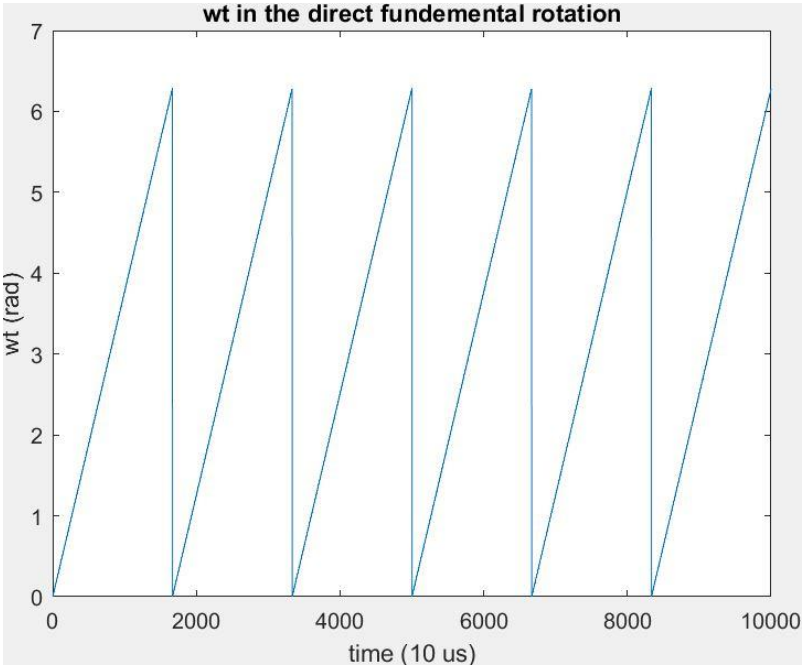

Figure 14. ωt in the direct fundemental rotation.

The synchronous reference frame can be made to rotate at the inverse fundamental frequency simply by inversing the values of the ramp signal, as can be seen in fig. 15, with no need for any extra components or calculations.

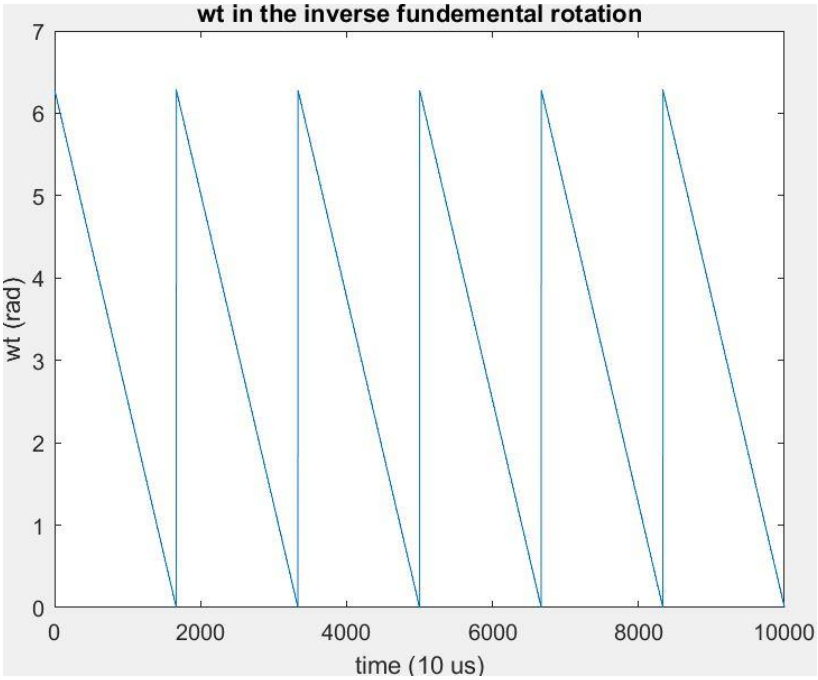

Figure 15. ωt in the inverse fundemental rotation.

By avoiding decoupling the positive and negative sequences, only two R-controller are used – one for Vd control and the other Vq control, where Vd and Vq are direct and quadrature components of the load voltage respectively. The Bode plots for the two R-controllers are shown in Fig. 16.

The transfer function of the R-filter is:

$$\frac{\mathrm{kr}}{s^2+\omega_2^2} \qquad (14)$$

Where kr is the gain of the R controller and ω_2 is the angular second harmonic.

The transfer function of the PI controller is:

$$\frac{\mathrm{kp}.s+\mathrm{ki}}{s} \qquad (15)$$

And hence, the complete transfer function of the voltage controller with the R-filter is:

$$\frac{\text{kp.s+ ki}}{s} + \frac{\text{kr}}{s^2+\omega_2^2} \quad (16)$$

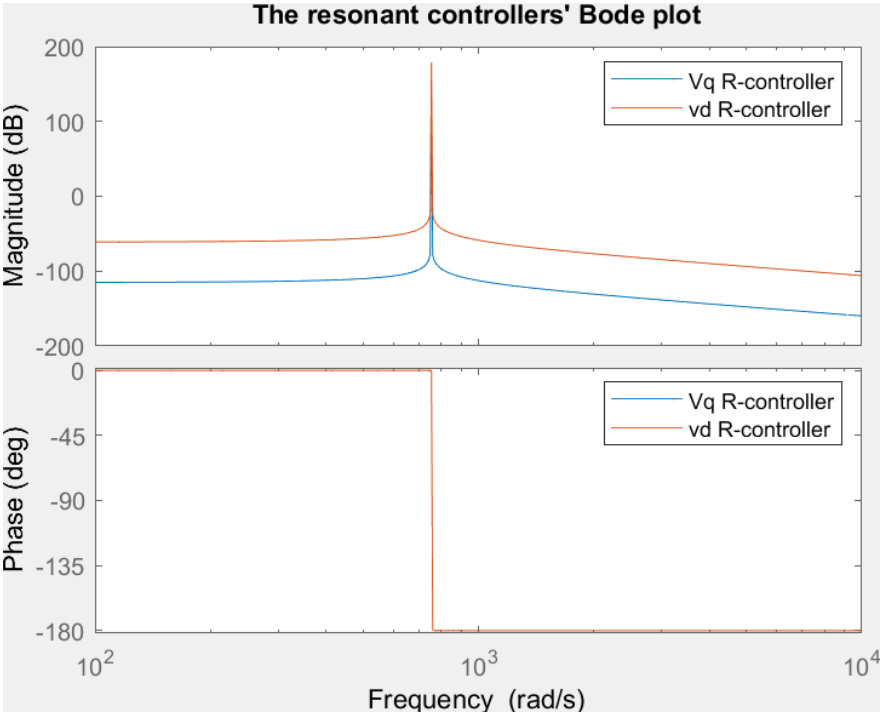

figure 16. The R-controllers' Bode Plot.

6.3 Standards for Important Voltage Regulation Parameters

[60] discusses the most prominent standards. It mentions that EN 50160 standards sets the limits some important design parameters as follows:

Maximum voltage THD is 8 %.

Maximum 3rd voltage harmonic level is 5%.

Maximum 3rd voltage harmonic level 6%.

Maximum 3rd voltage harmonic level 5%.

Voltage unbalance for three-phase inverters. Maximum unbalance is 3 %.

Voltage amplitude variations: maximum ±10 %.

Frequency variations: maximum ±1 %.

While IEEE 519-2014 sets a limit of 8% for the voltage THD and 5% for individual harmonics for $V \geq 1.0kV$, and a limit of 5% for voltage THD and 3% for individual harmonics for $1kV < V \leq 69kV$ – [61].

6.4 Summary

This chapter introduced another proposal which complements the main proposal, namely, a resonant controller tuned to the second harmonic while the d-q reference frame rotates at the inverse fundamental frequency. Some of the relevant standards are discussed. The proposed method is effective in balancing load voltage and the voltage harmonics are kept within the permitted levels, while using only two R-controllers. A comparative analysis of methods to regulate the voltage in unbalanced loads conditions were provided in the introduction section.

Chapter 7

Simulation

7.1 Simulation Set Up

Seven case studies are presented in this chapter. Case studies 1, 2, and 3 were devised and presented below to illustrate the main features of the SST, thereby validating the unified control strategy. Case studies 4 and 5 demonstrate two more proposals, namely the LVRT functionality and the harmonic mitigation method which validates the versatility of the unified control strategy as well as validates those individual proposals. Case study 6 presents the voltage regulation results for the proposed R-controller presented in the previous chapter. Case study 7 contrasts the proposed R-controller with the case when it is implemented in a d-q reference frame rotating at the direct fundamental frequency in terms of harmonics.

The system discussed in chapter 4 was built in Simulink and the main algorithm is implemented as one MATLAB function. A time step size of 1 micro-second was used. The simulation is high fidelity since Simulink is a real-time software. In fact, since simulation takes place over a period in the order of tenths of a second, the transient effects resulting from changing the values of different parameters is magnified many times and therefore it makes for a tougher environment than in

a real-life system. However, it is a good practice to test new proposals in real-life situations, but that is left for future work.

7.2 Case study 1 - Seamless Transition Between Modes of Operation

A smooth transition between the islanded and the grid-tied modes is one of the main requirements in a system such as the one in discussion - to guarantee a smooth and a safe operation. In this case study, the main parameter selected for observation is the load voltage through which the smooth transition can be verified. However, because the transition can happen at different PV power levels, this scenario is also examined. The BESS is used to help with regulating the load voltage in varying solar power levels. Therefore, those three parameters are presented for observation in Fig. 17.

In that figure, a three-phase breaker disconnects the grid at 0.05 seconds. The islanded mode control is triggered by the detection of zero grid current, and the control parameters are updated. The PV power is decreasing, but the battery is controlled through the main algorithm so that it allows the load to have the right amount of power. The grid is reconnected at 0.2 seconds. The load voltage level is regulated to match that of the grid voltage, thus achieving a seamless transfer between the two modes.

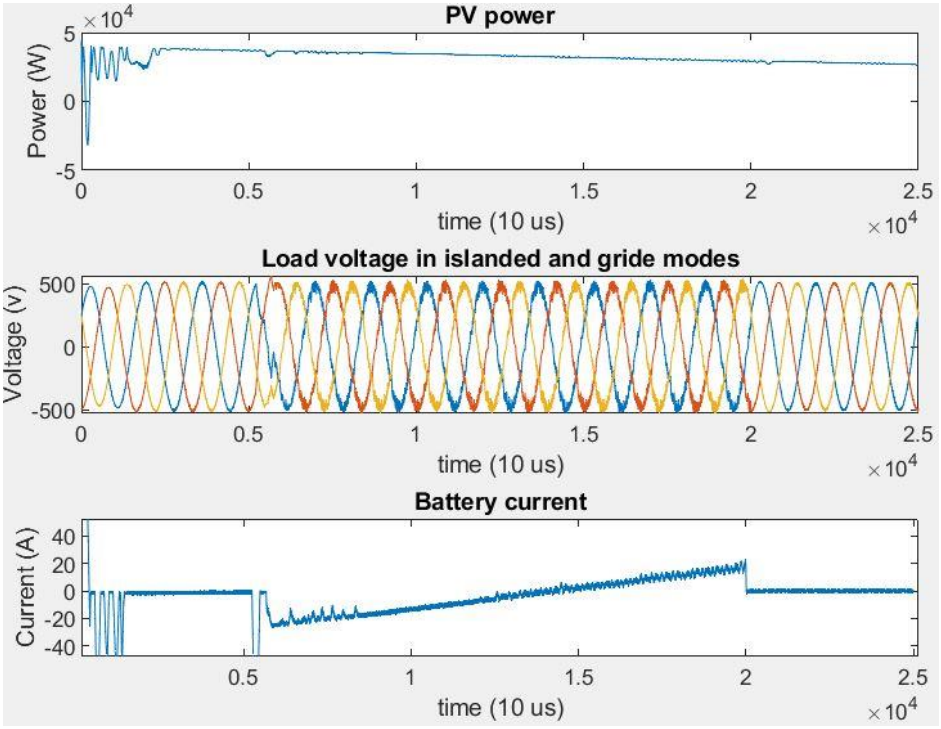

Figure 17. The seamless transfer between modes - Top: PV power, Middle: Load voltage, Bottom: Battery current.

7.3 Case Study 2 - Peak-Shaving

Peak shaving is a desirable function in power systems, specially in DGs, since it helps increase the efficiency of power generation. The main component which performs peak shaving is the BESS. The energy which the battery injects into the grid will show itself as inverter current as well as batter current. The PV power profile determines the profile of inverter current if no other input is considered, i.e., the battery current. Therefore, those are the parameters which are being investigated. They are presented in Fig. 18 and described as follows.

The filter current is decreasing linearly, reflecting the decrease in solar power. The on-peak period is defined in the main algorithm to be from 0.1 seconds to 0.35

seconds. The battery is discharging into the grid, and its current is superimposed on the PV boost converter current during the on-peak period. At the end of the on-peak period, the battery is not allowed to resume its charging state since the PV power is low, and that would lower the inverter current and increase the harmonic distortion.

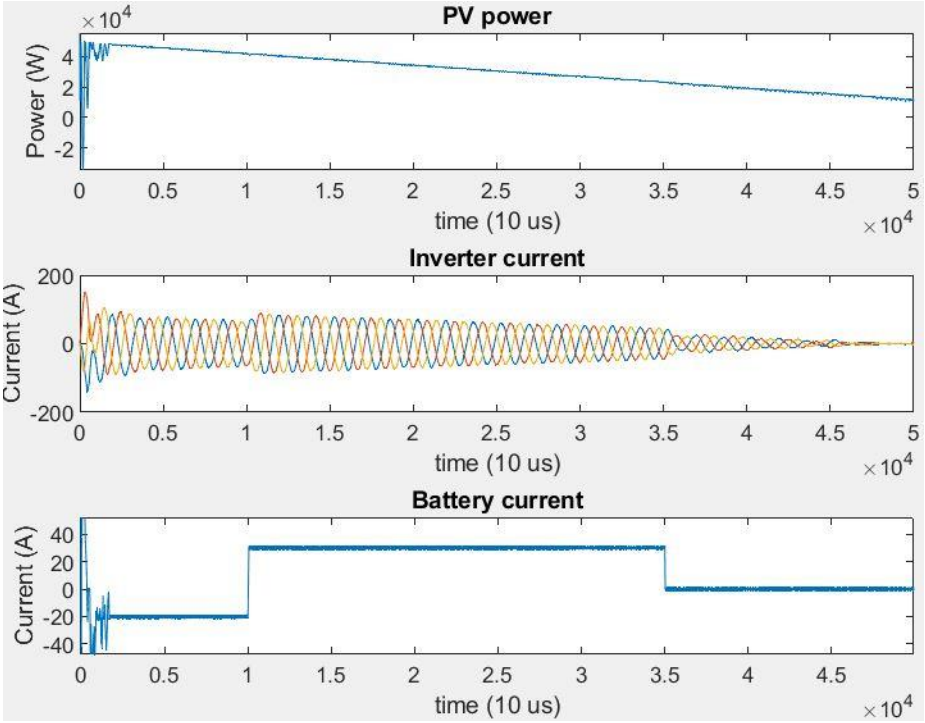

Figure 18. Peak-shaving - Top: PV power, Middle: Inverter current, Bottom: Battery current.

7.4 Case Study 3- SST Bidirectionality

The BESS should be able to serve as energy back up. However, if there isn't enough solar power available to charge the battery to a safe level, then the H-Bridge should be controlled such that it reverses the direction of power flow thereby

allowing the battery to charge from the grid. To prove the correct operation of that scenario, the battery should be shown to charge, the inverter current should correspond to the charging of the battery, and the solar power should be shown to have no input in that charging process. Therefore, those parameters are presented in Fig. 19 for analysis as follows.

The solar power is decreasing. The battery is not allowed to charge any more to reduce the harmonic distortion. The low current is suppressed by the proposed THD improvement method. As per the algorithm, the H-bridge reverses the direction of power to allow the grid to charge the battery to a level that allows it to serve as a power backup in case the grid gets disconnected. The battery is shown to charge while the solar power is zero, indicating that the source of power is the grid.

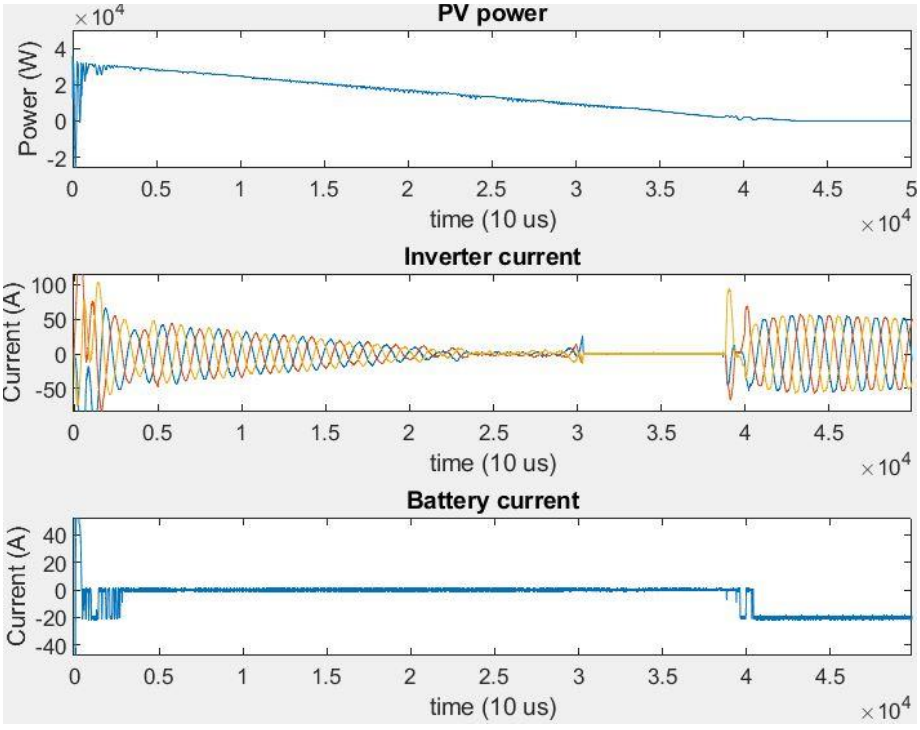

figure 19. The SST bidirectionality - Top: PV power, Middle: Inverter current, Bottom: Battery current.

7.5 Case Study 4 - LVRT

The proposed LVRT method is a stand-alone proposal. It also serves as a way to validate the versatility of the proposed unified control strategy and hence, it was important to develop a case study for it. The test parameters are the solar power which would indicate the status of the MPPT, the inverter current and the grid voltage plotted on one figure to show the successful injection of the required reactive power into the grid through the phase shift, the battery current and the inverter current to show how the inverter current is successfully limited to its rated value.

The E. ON LVRT requirements which are presented in [44] are used as an example to test the proposed LVRT algorithm. The model discussed earlier was built in Simulink. The irradiance was set at a high value of 1000 to guarantee excess power and therefore test whether the BESS can absorb that power to protect the inverter. A 3-phase ground fault through a resistor was created at critical load which is parallel to the grid connection at time 0.05 seconds and cleared at time 0.1 seconds.

The simulation results in Fig. 20 and Fig 21 show the grid current is in phase with voltage before and after the fault, but it leads the voltage during the voltage sag, thereby injecting reactive current into the grid – only phase c is shown for better visibility - and the algorithm is able to provide the correct the battery reference current to the controller of the BESS allowing the battery to absorb the excess power and keeping the inverter current below its rated value which is specified in the algorithm as 110 (A).

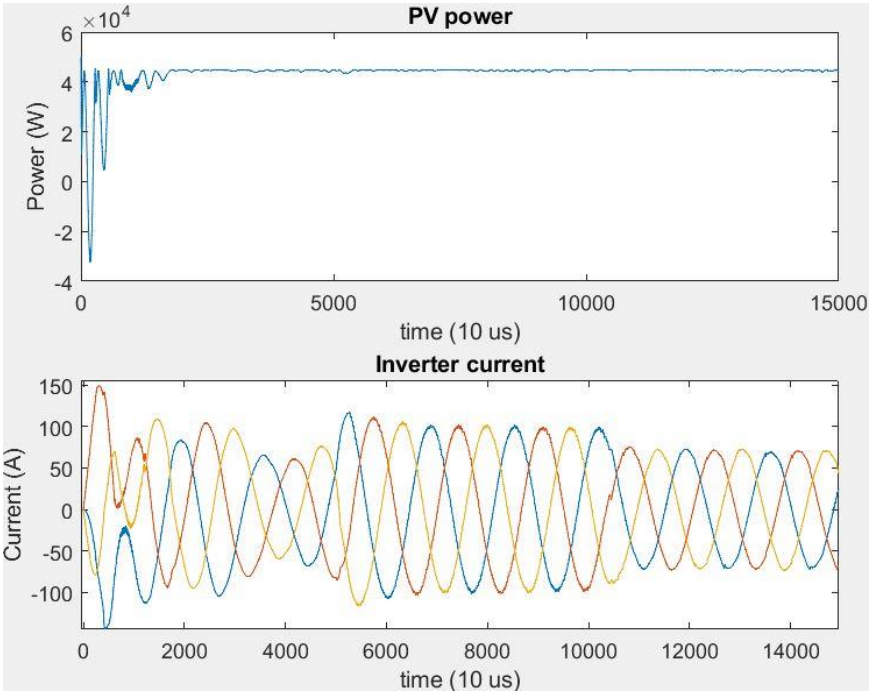

figure 20. LVRT - Top: Inverter current, Bottom: Battery current.

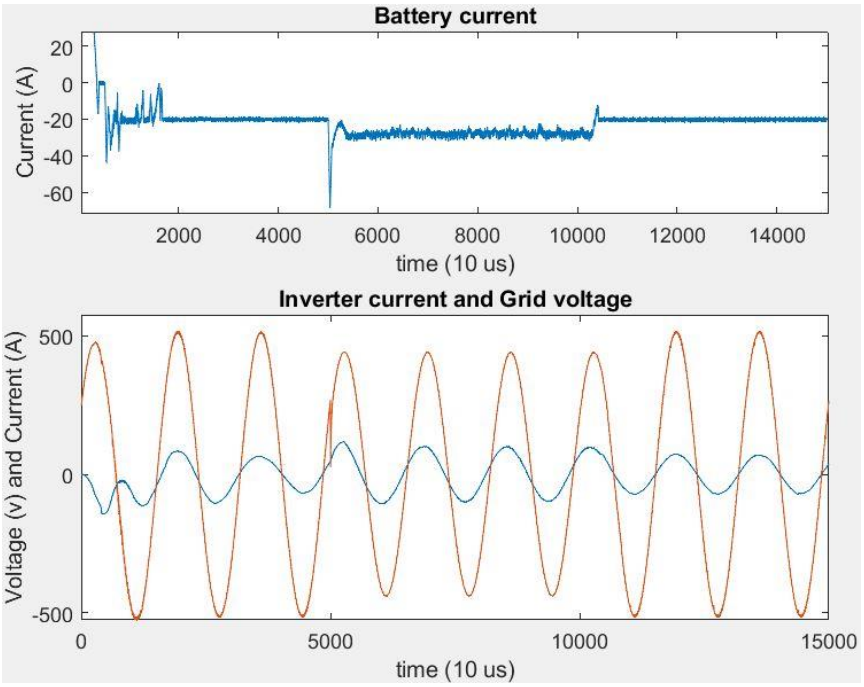

figure 21. LVRT, Top: PV power, Bottom: Grid voltage and current (phase a).

7.6 Case Study 5 - Harmonic Distortion Mitigation

The proposed harmonic distortion mitigation function is an original way of mitigating harmonic distortion, and it is necessary to demonstrate that in this work. The inverter current and its harmonics are the only parameters needed for this demo. The result is contrasted with the same case without the proposed method for comparison in Fig 22 and Fig 23.

In both figures, the solar power is made to decrease linearly. At high PV power indicated by the higher current side, the reference voltage is chosen to be slightly higher than the grid voltage plus the voltage across the filter. A lower reference voltage would result in controller saturation. As the filter current decreases, so does the voltage across the filter, and so the reference voltage is lowered by the algorithm without causing the controller to saturate, thereby increasing the current and reducing the harmonic distortion as can be observed around 0.27 seconds. When the PV power and, therefore the inverter current is noticeably low, the algorithm increases the reference voltage to reduce the current even further. This happens at time 0.44 sec. The Kp values had to be adjusted. Fig. 23 represents the same scenario without the THD improvement method. It can be seen in fig. 22 and fig. 23 that the proposed method results in THD reduction from 15% to 8% at medium to low PV power and from around 70% to around 3% at very low PV power. The power levels at which the reference voltage is changed are chosen according to the corresponding values of THD.

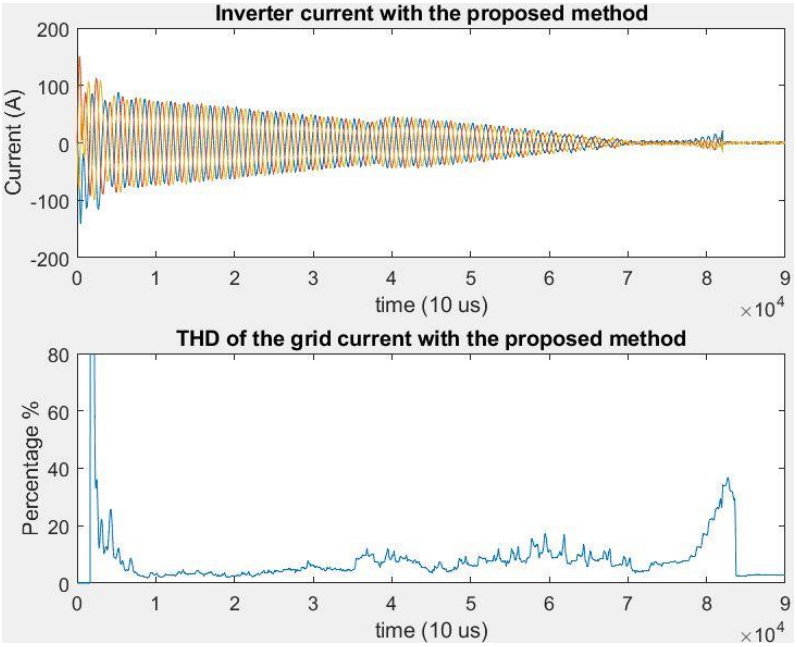

figure 22. Improved THD - Top: Inverter current, Bottom: Grid current THD.

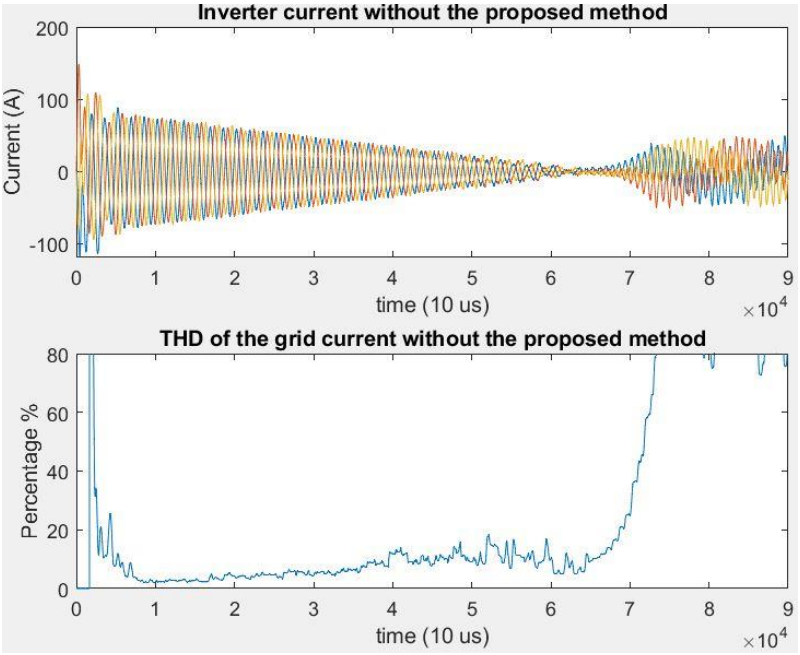

Figure 23. THD without the proposed method- Top: Inverter current, Bottom: Grid current THD.

7.7 Case Study 6 – Unbalanced Load

The purpose of this case study is to validate the fourth proposal of this research, namely the R-filter. The load voltage is the main parameter required to demo the performance of the R-filter, but the load current is also needed to show the state of load i.e., it being unbalanced. This is contrasted with the case without the proposed R-filter for comparison in fig. 24 and fig. 25.

The higher current in one of the phases in fig. 24 and fig. 25 indicates unbalanced load conditions. This was simulated using a 5-Ohm resistance in that phase and two 20-Ohm resistances in each of the other two phases. The voltage is unbalanced in fig. 24. The R-controllers for Vd and Vq, given by the Bode plots in fig. 16 are then connected as per fig. 13. As a result, the voltage can be seen balanced in fig. 25.

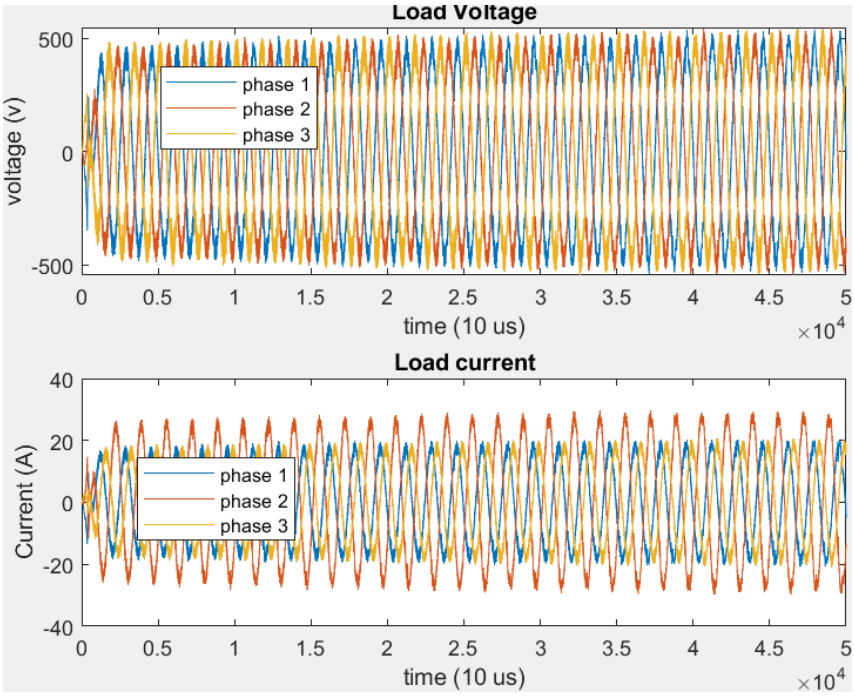

Figure 24. Balanced voltage in unbalanced load condition.

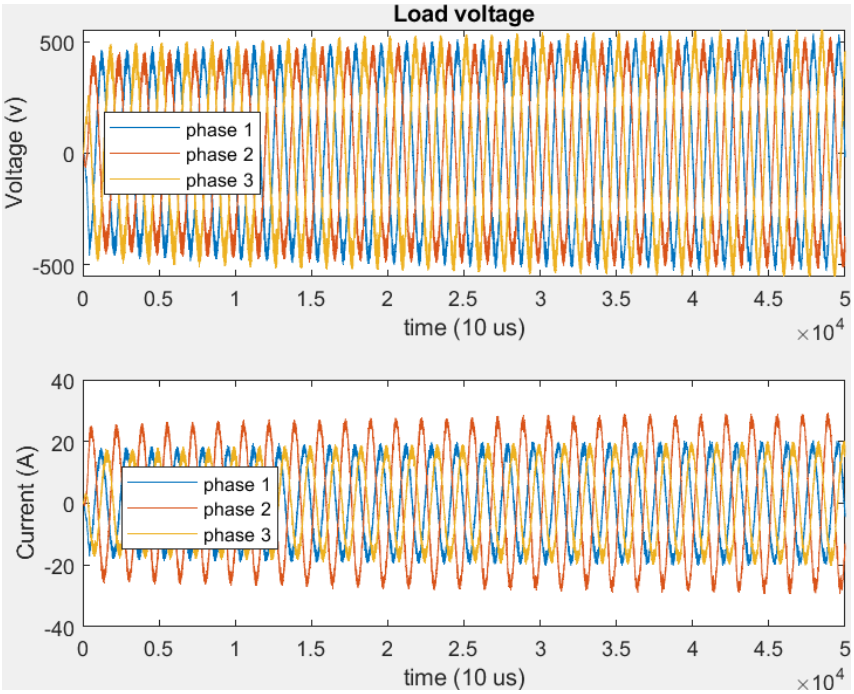

Figure 25. Unbalanced load condition without balancing measures.

7.8 Case Study 7 – R-controllers' Harmonics Comparison

As discussed in chapter 6, [56] proposes a resonant controller to compensate for the 2nd harmonic in the d-q reference frame, but it is used in the direct fundamental d-q reference frame. It also proposes two more compensators for the harmonics caused by non-linear loads which are tuned to the 6th and the 12th harmonics. This case study is devised to show that extra filters besides the ones tuned for the 2nd harmonic would be needed in this case even if no non-linear loads were connected to the system and that filtering the 2nd harmonic this way would create more harmonics namely, the inverse 5th and the direct 7th.

Fig. 26 shows the result of that the proposed method. Ignoring the transient effects, all the main harmonics are shown to be withing the 3% limit given by IEEE 519-2014 standards. The fundamental component - now the inverse fundamental since the rotation is in the opposite direction – is off the scale to allow for better visibility for the levels of the other harmonics. The other method, on the other hand, results in high inverse 5^{th} and direct 7^{th} harmonics as can be seen in fig. 27. It is the direct fundamental that is off the scale there since it is the main component in the direct rotation. The voltage regulation results of that method are shown in fig. 28. The voltage is balanced. However, it does not appear balanced as it should due to the large harmonic spikes.

The results validate the reason for implementing the R-controller in the inverse fundamental rotation d-q reference frame as per the proposed method presented in chapter 6.

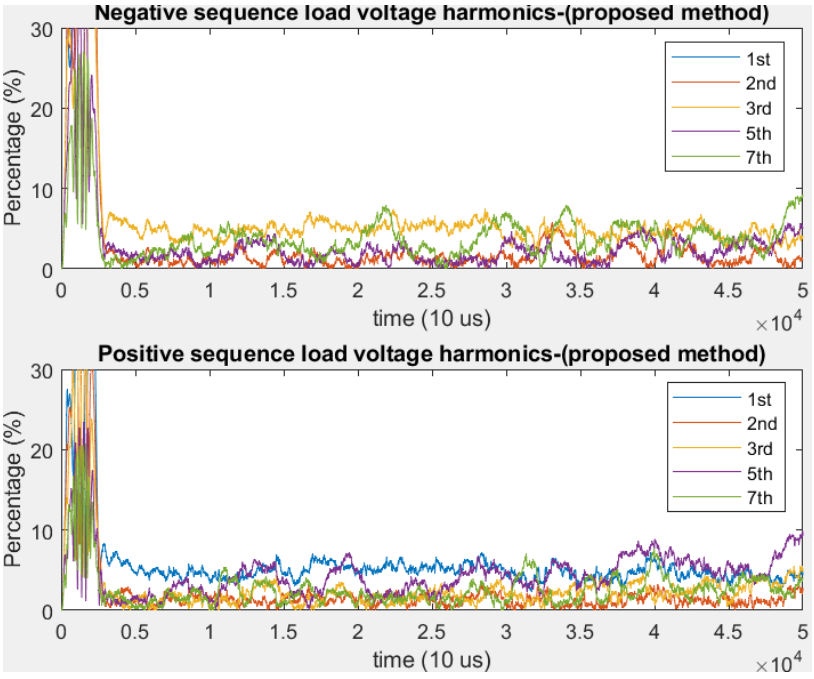

Figure 26. The voltage harmonics in the proposed R-controller method. The inverse fundamental is off the scale.

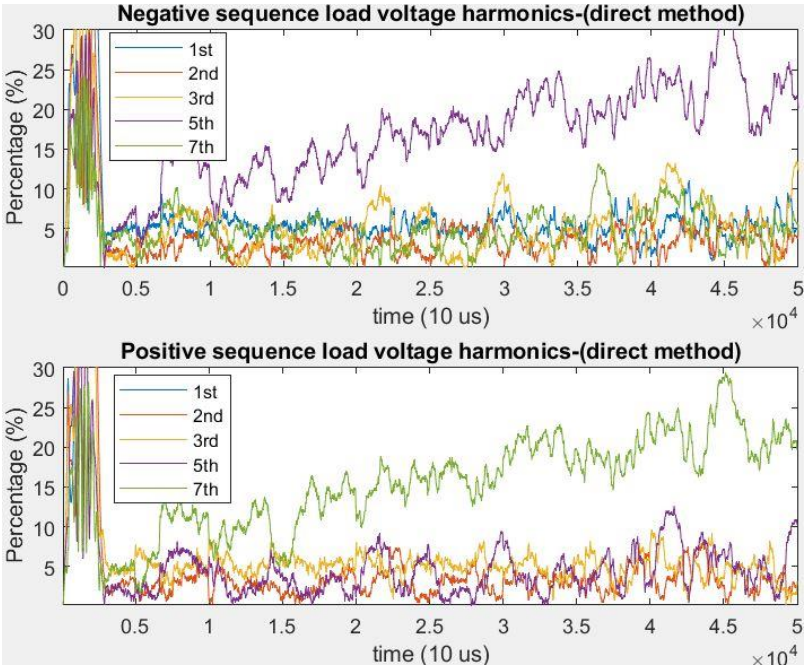

Figure 27. The voltage harmonics in the R-controller with direct rotation. The direct fundamental is off the scale.

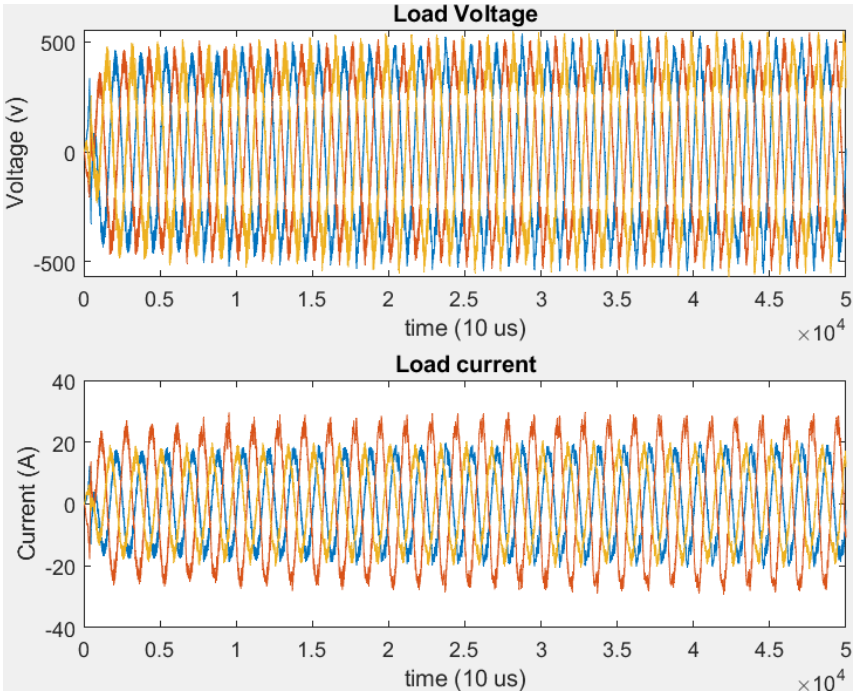

Figure 28. The voltage harmonic distortion in the R-filter with direct rotation.

7.9 Summary

This chapter presented seven case studies were simulated in Simulink. Case studies 1, 2, and 3 illustrated the main features of the SST, thereby validating the unified control strategy. Case studies 4, 5, 6, and 7 demonstrated three more proposals, namely the LVRT functionality, the harmonic mitigation method, and the proposed R-controller presented which further validates the control strategy and highlights its versatility. Further case studies should also be devised to examine the system behaviour during load variations and during various faults which left for future work.

Chapter 8

Conclusions and Future Work

8.1 Conclusion

Research proposing a unified control strategy for SST has been presented in this report. The control strategy is designed to be comprehensive, yet compact and offer a good and a convenient infrastructure for future modifications. The control of all stages of the SST is managed in one function where the inter-connectivity of all the SST stages is considered. This proposal gave rise to three more proposals which have also been presented here. Namely, an efficient LVRT scheme, a software-based harmonic mitigation method, and a resonant controller in the inverse fundamental d-q reference frame to help regulate the load voltage in islanded mode in unbalanced load conditions. Those proposals aim to compliment the control strategy and illustrate its versatility and efficiency.

It is important to give a solid background to the main research and so, after giving a brief introduction in chapter 1, chapter 2 provided a comprehensive overview of the SST's physical structure and topologies. A general description of the SST control was also presented; however, chapter 3 expands on the control of the SST - particularly the inverter control and the BESS control - given the relevance of that to this research.

The proposed system and the unified control strategy were presented in chapter 4 – highlighting the originality and uniqueness of the proposed control strategy and how it considers the interdependency of all the stages of the SST to achieve better organization and efficiency - whereas previous literature on SST control have failed to do so.

The proposed LVRT and the harmonic distortion mitigation methods were presented in chapter 5, while the resonant controller proposal was presented in chapter 6. The most relevant literature review was presented in chapters 2, 3, 5 and 6 - as per the presented topic. In terms or LVRT, the proposal has been shown to be highly efficient in comparison with the reviewed strategies. As to the harmonic distortion mitigation proposal, it is clearly original, in that, it is software-based whereas other harmonic distortion mitigation methods have been hardware-based. This, of course, improves the quality of the system without the use of any extra hardware which translates to lower cost. This is new approach of harmonic distortion mitigation which was possible only because of the infrastructure which the proposed control strategy offers. The proposal voltage regulation in unbalanced load condition was also contrasted with previous work and found to be superior since it only uses fewer filters used in that other paper with no trade-offs as explained in section 7.8.

The standards for the most relevant design parameters were presented in chapter 6 to demonstrate the proposals ability to meet the standards.

Seven case studies were devised and conducted in Simulink. The simulation results were presented in chapter 7. The proposed resonant controller was shown to achieve balanced voltage in unbalanced load conditions and satisfy the standards in terms of levels of harmonics, voltage imbalance and voltage variations. The LVRT method was demonstrated to be efficient for several reasons as discussed in

chapter 5. The harmonic distortion mitigation method results in THD reduction from 15% to 8% at medium to low PV power and from around 70% to around 3% at very low PV power. The proposed R-filter for voltage regulation in unbalanced load conditions has been shown to provide balanced voltage regulation while maintaining an acceptable level of harmonics as per the standards which were also presented in this report. And hence, all the proposals have been verified as described and the main unified control strategy has been demonstrated to be effective and efficient.

8.2 The Applicability and Safety Considerations

As discussed in section 4.1, the SST starts from the DC link at the output of the PV DC/DC converter. It does not see what is behind that – whether it is a PV, a wind turbine, or otherwise. Therefore, the applicability of the proposals of this research are not limited by the specific type of the DG.

Furthermore, there is no limitations in terms of scale. The system can be scaled up and, although it might be obvious that the hardware configuration will be affected and a careful analysis will be needed to determine the exact limitations, since the proposals are software solutions, they will not be affected by scalability and the resulting change in hardware configuration. The concepts and the main algorithm will still apply. However, some specifics will need adjusting. For example, the algorithm outputs the various gate signals depending on the present case and so, if the number of switches change because of scalability then that needs to be reflected in the code.

The safety considerations of power systems are established, and requirements and standards are provided in the applicable standards to ensure the safe operation of the system - as discussed in section 6.3 for example. LVRT

requirements, for another example, ensure the stability of the power system as well as the protection of the inverter. The proposals of this research do not, in and of themselves, create safety issues given their software nature. However, the proposals do, as they must, comply with all the applicable requirements and standards.

8.3 Future Work

- Future work regarding the proposed unified control strategy should include investigating the system behaviour with non-linear loads and subsequently propose mitigation method/s for dealing with the harmonics created as a result of the non-linear load.

- More case studies could be performed to investigate the behaviour of the system in various kinds of faults and load variations.

- As previously discussed, the proposed unified control strategy design started with inverter control schemes which had their limitations. Future work research can investigate taking the same approach of the proposed unified control strategy but use a more advanced inverter control schemes as the starting point. Favourable results could be used to establish the generality of the proposed unified control scheme. Another good objective is to investigate whether the unified control strategy can be used to simplify existing such schemes.

- The versatility of the proposed unified control strategy means that it could extend beyond the control of the SST and to the DG and its converter be that solar or wind power generation, and so that would be a viable future research topic.

- Future work should include testing the proposals in a real-life system.

- Other possible future research is to test the proposed control strategy in wind power setting. This does not seem to be an urgent topic since the distributed generation is not considered to be part of the SST or its control. However, as discussed in the third bullet point here, it is possible that the proposed unified control strategy is used to simplify the DG, in which case it would be a good idea to investigate that proposal in a wind power setting.

References

[1] M. A. Hannan, Pin Jern Ker, Molla S. Hossain Lipu, Zhen Hang Choi, M. Safwan Abd. Rahman, Kashem M. Muttaqi, Frede Blaabjerg, “State of the Art of Solid-State Transformers: Advanced Topologies, Implementation Issues, Recent Progress and Improvements,” IEEE Access, Vol. 8, Jan. 2020.

[2] M. A. Shamshuddin, F. Rojas, R. Cardenas, J. Pereda, M. Diaz, R. Kennel, “Solid State Transformers: Concepts, Classification, and Control,” Energies, Vol. 13(9), May 2020.

[3] X. She, A. Huang, “Solid state transformer in the future smart electrical system,” 2013 IEEE Power Energy Society General Meeting, 2013, pp. 1-5, doi: 10.1109/PESMG.2013.6672768.

[4] J. E. Huber and J. W. Kolar, “Applicability of Solid-State Transformers in Today’s and Future Distribution Grids,” in IEEE Transactions on Smart Grid, vol. 10, no. 1, pp. 317-326, Jan. 2019, doi: 10.1109/TSG.2017.2738610.

[5] D. Ronanki and S. S. Williamson, “Evolution of Power Converter Topologies and Technical Considerations of Power Electronic TransformerBased Rolling Stock Architectures,” in IEEE Transactions on Transportation Electrification, vol. 4, no. 1, pp. 211-219, March 2018, doi: 10.1109/TTE.2017.2765518.

[6] S. A. Saleh, Emre Ozkop, Basim Alsayid, Chistian Richard, Xavier Francis St. Onge, Katie M. McDonald, Liuchen Chang, “Solid-State Transformers for

Distribution Systems–Part II: Deployment Challenges," in IEEE Transactions on Industry Applications, vol. 55, no. 6, pp. 5708- 5716, Nov.-Dec. 2019, doi: 10.1109/TIA.2019.2938143.

[7] Agheb, E.; Høidalen, H.K. Medium frequency high power transformers, state of art and challenges. In Proceedings of the 2012 International conference on renewable energy research and applications (ICRERA), Nagasaki, Japan, 11–14 November 2012; IEEE: Hoboken, NJ, USA, 2012; pp. 1–6.

[8] M. Mogorovic and D. Dujic, "Sensitivity Analysis of MediumFrequency Transformer Designs for Solid-State Transformers," in IEEE Transactions on Power Electronics, vol. 34, no. 9, pp. 8356-8367, Sept. 2019, doi: 10.1109/TPEL.2018.2883390.

[9] R. Agarwal, S. Martin and H. Li, "Influence of Phase-Shifted Square Wave Modulation on Medium Frequency Transformer in a MMC Based SST," in IEEE Access, vol. 8, pp. 221093-221102, 2020, doi: 10.1109/ACCESS.2020.3042935.

[10] T. O. Olowu, H. Jafari, M. Moghaddami and A. I. Sarwat, "Multiphysics and Multiobjective Design Optimization of High-Frequency Transformers for Solid-State Transformer Applications," in IEEE Transactions on 5 Industry Applications, vol. 57, no. 1, pp. 1014-1023, Jan.-Feb. 2021, doi: 10.1109/TIA.2020.3035129.

[11] M. Ghassemi, "Accelerated insulation aging due to fast, repetitive voltages: A review identifying challenges and future research needs," in IEEE Transactions on

Dielectrics and Electrical Insulation, vol. 26, no. 5, pp. 1558-1568, Oct. 2019, doi: 10.1109/TDEI.2019.008176.

[12] S. Zengin and M. Boztepe, “Trapezoid current modulated DCM AC/DC DAB converter for two-stage solid state transformer,” 2015 9th International Conference on Electrical and Electronics Engineering (ELECO), 2015, pp. 634-638, doi: 10.1109/ELECO.2015.7394538.

[13] T. Besselmann, A. Mester and D. Dujic, “Power Electronic Traction Transformer: Efficiency Improvements Under Light-Load Conditions,” in IEEE Transactions on Power Electronics, vol. 29, no. 8, pp. 3971-3981, Aug. 2014, doi: 10.1109/TPEL.2013.2293402.

[14] L. Zheng, R. P. Kandula and D. Divan, “Soft-Switching Solid-State Transformer With Reduced Conduction Loss,” in IEEE Transactions on Power Electronics, vol. 36, no. 5, pp. 5236-5249, May 2021, doi: 10.1109/TPEL.2020.3030795.

[15] Y. Liu, Y. Liu, B. Ge and H. Abu-Rub, “Interactive Grid Interfacing System by Matrix-Converter-Based Solid State Transformer With Model Predictive Control,” in IEEE Transactions on Industrial Informatics, vol. 16, no. 4, pp. 2533-2541, April 2020, doi: 10.1109/TII.2017.2679137.

[16] L. Zheng, R. P. Kandula and D. Divan, “Robust Predictive Control for Modular Solid-State Transformer With Reduced DC Link and Parameter Mismatch,” in IEEE

Transactions on Power Electronics, vol. 36, no. 12, pp. 14295-14311, Dec. 2021, doi: 10.1109/TPEL.2021.3085679.

[17] H. Wen, J. Gong, C. Yeh, Y. Han and J. Lai, “An Investigation on Fully Zero-Voltage-Switching Condition for High-Frequency GaN Based LLC Converter in Solid-State-Transformer Application,” 2019 IEEE Applied Power Electronics Conference and Exposition (APEC), 2019, pp. 797- 801, doi: 10.1109/APEC.2019.8721789.

[18] M. Rashidi, N. N. Altin, S. S. Ozdemir, A. Bani-Ahmed and A. Nasiri, “Design and Development of a High-Frequency Multiport Solid-State Transformer With Decoupled Control Scheme,” in IEEE Transactions on Industry Applications, vol. 55, no. 6, pp. 7515-7526, Nov.-Dec. 2019, doi: 10.1109/TIA.2019.2939741.

[19] H. Wang, Yichun Zhang, Yao Sun, Minghui Zheng, Xiao Liang, Guanguan Zhang, Kaiyuan Tan, Jianghua Feng, “Topology and Control Method of a Single-Cell Matrix-Type Solid-State Transformer,” in IEEE Journal of Emerging and Selected Topics in Power Electronics, vol. 8, no. 3, pp. 2302-2312, Sept. 2020, doi: 10.1109/JESTPE.2019.2940514.

[20] R. Jaiswal, V. Mittal, A. Agrawal and V. Agrawal, “Voltage and Power Balance of a Three-phase Solid State Transformer using A Decoupled Control Strategy for Grid-Side Converter,” 2018 International Conference on Computing, Power and Communication Technologies (GUCON), 2018, pp. 445-450, doi: 10.1109/GUCON.2018.8675119.

[21] Verma, Neevatika Singh, Dr. Navdeep Yadav, Shekhar Gupta, Sandeep. (2018). Reactive Power Compensation of Solid State Transformer for WECS. 1-6. 10.1109/IEMENTECH.2018.8465278.

[22] (F. Mohammadi, Behnam Mohammadi-Ivatloo, Gevork B. Gharehpetian, Mohd. Hasan Ali, Wei Wei, Ozan Erdinç, Mohammadamin Shirkhani, "Robust Control Strategies for Microgrids: A Review," in IEEE Systems Journal, doi: 10.1109/JSYST.2021.3077213.

[23] R. Tirumala, N. Mohan and C. Henze, "Seamless transfer off gridconnected PWM inverters between utility-interactive and stand-alone modes," APEC. Seventeenth Annual IEEE Applied Power Electronics Conference and Exposition (Cat. No.02CH37335), 2002, pp. 1081-1086 vol.2, doi: 10.1109/APEC.2002.989378.

[24] Z. Yao, L. Xiao and Y. Yan, "Seamless Transfer of Single-Phase GridInteractive Inverters Between Grid-Connected and Stand-Alone Modes," in IEEE Transactions on Power Electronics, vol. 25, no. 6, pp. 1597-1603, June 2010, doi: 10.1109/TPEL.2009.2039357.

[25] X. Meng, J. Liu, Z. Liu and R. An, "An Improved Droop Control Based Smooth Transfer Control Strategy," 2018 International Power Electronics Conference (IPEC-Niigata 2018 -ECCE Asia), 2018, pp. 957-962, doi: 10.23919/IPEC.2018.8507854.

[26] Z. Liu, J. Liu and Y. Zhao, “A Unified Control Strategy for Three-Phase Inverter in Distributed Generation,” in IEEE Transactions on Power Electronics, vol. 29, no. 3, pp. 1176-1191, March 2014, doi:10.1109/TPEL.2013.2262078.

[27] K. Zhang, Guanrui Wang, Xin Geng, Songjie Hu, Juan Liu, Zihao Jia, Xiaoyu Ai, Xihang Yang, “A Seamless Soft Transferring Method for Microgrid Energy Storage Converter,” 2021 13th International Conference on Measuring Technology and Mechatronics Automation (ICMTMA), 2021, pp. 150-154, doi: 10.1109/ICMTMA52658.2021.00041.

[28] M. Zhou, H. Liu, W. Wang and F. Blaabjerg, “Seamless Transfer Scheme Based on Unified Control Structure for Single-Stage Photovoltaic Inverter,” 2019 22nd International Conference on Electrical Machines and Systems (ICEMS), 2019, pp. 1-5, doi: 10.1109/ICEMS.2019.8922300.

[29] Briz, F.; Lopez, M.; Rodriguez, A.; Arias, M. Modular power electronic transformers: Modular multilevel converter versus cascaded H-bridge solutions. IEEE Ind. Electron. Mag. 2016, 10, 6–19.

[30] R. Tirumala, N. Mohan and C. Henze, “Seamless transfer off gridconnected PWM inverters between utility-interactive and stand-alone modes,” APEC. Seventeenth Annual IEEE Applied Power Electronics Conference and Exposition (Cat. No.02CH37335), 2002, pp. 1081-1086 vol.2, doi: 10.1109/APEC.2002.989378.

[31] Z. Yao, L. Xiao and Y. Yan, “Seamless Transfer of Single-Phase GridInteractive Inverters Between Grid-Connected and Stand-Alone Modes,” in IEEE Transactions on Power Electronics, vol. 25, no. 6, pp. 1597-1603, June 2010, doi: 10.1109/TPEL.2009.2039357.

[32] X. Meng, J. Liu, Z. Liu and R. An, “An Improved Droop Control Based Smooth Transfer Control Strategy,” 2018 International Power Electronics Conference (IPEC-Niigata 2018 -ECCE Asia), 2018, pp. 957-962, doi: 10.23919/IPEC.2018.8507854.

[33] Z. Liu, J. Liu and Y. Zhao, “A Unified Control Strategy for Three-Phase Inverter in Distributed Generation,” IEEE Transactions on Power Electronics, vol. 29, no. 3, pp. 1176-1191, March 2014, doi:10.1109/TPEL.2013.2262078.

[34] K. Zhang, Guanrui Wang, Xin Geng, Songjie Hu, Juan Liu, Zihao Jia, Xiaoyu Ai, Xihang Yang, “A Seamless Soft Transferring Method for Microgrid Energy Storage Converter,” 2021 13th International Conference on Measuring Technology and Mechatronics Automation (ICMTMA), 2021, pp. 150-154, doi: 10.1109/ICMTMA52658.2021.00041.

[35] M. Zhou, H. Liu, W. Wang and F. Blaabjerg, “Seamless Transfer Scheme Based on Unified Control Structure for Single-Stage Photovoltaic Inverter,” 2019 22nd International Conference on Electrical Machines and Systems (ICEMS), 2019, pp. 1-5, doi: 10.1109/ICEMS.2019.8922300.

[36] F. Mohammadi et al., “An improved droop-based control strategy for MTHVDC systems,” Electron., vol. 9, no. 1, Jan. 2020.

[37] J. Salaet, S. Alepuz, A. Gilabert and J. Bordonau, “Comparison between two methods of DQ transformation for single phase converters control. Application to a 3-level boost rectifier,” 2004 IEEE 35th Annual Power Electronics Specialists Conference (IEEE Cat. No.04CH37551), 2004, pp. 214-220 Vol.1, doi: 10.1109/PESC.2004.1355744.

[38] U. A. Miranda, L. G. B. Rolim and M. Aredes, “A DQ Synchronous Reference Frame Current Control for Single-Phase Converters,” 2005 IEEE 36th Power Electronics Specialists Conference, 2005, pp. 1377- 1381, doi: 10.1109/PESC.2005.1581809.

[39] B. Bereczki, B. Hartmann and S. Kertész, "Industrial Application of Battery Energy Storage Systems: Peak shaving," 2019 7th International Youth Conference on Energy (IYCE), 2019, pp. 1-5, doi: 10.1109/IYCE45807.2019.8991594.

[40] S. Sitompul and G. Fujita, "Implementation of BESS Load Frequency Control in Islanded Microgrid System by Considering SOC," 2020 IEEE PES Innovative Smart Grid Technologies Europe (ISGT-Europe), 2020, pp. 980-984, doi: 10.1109/ISGT-Europe47291.2020.9248945.

[41] K. Chatchairungruang and S. Suwankawin, "Peak-Shaving of Feed-in PV Power for Residential PV-Battery System with Added Feedback-Adjustment Scheme," 2021 18th International Conference on Electrical Engineering/Electronics,

Computer, Telecommunications and Information Technology (ECTI-CON), 2021, pp. 192- 195, doi: 10.1109/ECTI-CON51831.2021.9454817.

[42] N. Boyouk, N. Munzke and M. Hiller, "Peak Shaving of a Grid connected-Photovoltaic Battery System at Helmholtz Institute Ulm (HIU)," 2018 IEEE PES Innovative Smart Grid Technologies Conference Europe (ISGTEurope), 2018, pp. 1-5, doi: 10.1109/ISGTEurope.2018.8571616.

[43] R. Manojkumar, C. Kumar, S. Ganguly and J. P. S. Catalão, "Optimal Peak Shaving Control Using Dynamic Demand and Feed-In Limits for Grid-Connected PV Sources With Batteries," in IEEE Systems Journal, doi: 10.1109/JSYST.2020.3045020.

[44] Yong-Sih Wu, Chia-His Chang, Yaow-Ming Chen, Chih-Wen Liu and Yung-Ruei Chang, “A current control strategy for three-phase PV power system with low-voltage ride-through,” 9th IET International Conference on Advances in Power System Control, Operation and Management (APSCOM 2012), 2012, pp. 1-6, doi: 10.1049/cp.2012.2140.

[45] L. Yaoyuan, Z. Chengbi, M. Hong and F. Wenwen, “Research on a new method to achieve low voltage ride through of PV,” 2014 International Conference on Power System Technology, 2014, pp. 1628-1634, doi: 10.1109/POWERCON.2014.6993960

[46] P. N. Joshi and S. Dadaso Patil, “Improving low voltage ride through capabilities of grid connected residential solar PV system using reactive 5 power injection strategies,” 2017 International Conference on Technological

Advancements in Power and Energy (TAP Energy), 2017, pp. 1-3, doi: 10.1109/TAPENERGY.2017.8397301.

[47] F. -J. Lin, J. -C. Liao, C. -I. Chen, P. -R. Chen and Y. -M. Zhang, “Voltage Restoration Control for Microgrid With Recurrent Wavelet Petri Fuzzy Neural Network,” in IEEE Access, vol. 10, pp. 12510-12529, 2022, doi: 10.1109/ACCESS.2022.3147357.

[48] M. Y. Worku and M. A. Abido, “Grid-connected PV array with supercapacitor energy storage system for fault ride through,” 2015 IEEE International Conference on Industrial Technology (ICIT), 2015, pp. 2901-2906, doi: 10.1109/ICIT.2015.7125526.

[49] Rose-Hulman Institute of Technology. (n.d.). Lect15-Harmonics. Terre Haute, Indiana.

[50] Z. Liu, J. Liu and Y. Zhao, "A Unified Control Strategy for Three-Phase Inverter in Distributed Generation," in IEEE Transactions on Power Electronics, vol. 29, no. 3, pp. 1176-1191, March 2014, doi: 10.1109/TPEL.2013.2262078.

[51] H. Shi, F. Zhuo, H. Yi and Z. Geng, "Control strategy for microgrid under three-phase unbalance condition," in Journal of Modern Power Systems and Clean Energy, vol. 4, no. 1, pp. 94-102, January 2016, doi: 10.1007/s40565-015-0182-3.

[52] V. R. Chowdhury, S. Mukherjee, P. Shamsi and M. Ferdowsi, "Control of a three-phase inverter under unbalanced grid conditions," 2017 IEEE Energy

Conversion Congress and Exposition (ECCE), 2017, pp. 2909-2913, doi: 10.1109/ECCE.2017.8096537.

[53] T. D. C. Busarello, J. A. Pomilio and M. G. Simoes, "Design Procedure for a Digital Proportional-Resonant Current Controller in a Grid Connected Inverter," 2018 IEEE 4th Southern Power Electronics Conference (SPEC), 2018, pp. 1-8, doi: 10.1109/SPEC.2018.8636052.

[54] Teodorescu, R. & Blaabjerg, F. & Liserre, Marco & Loh, P.. (2006). Proportional-resonant controllers and filters for grid-connected voltage-source converters. Electric Power Applications, IEE Proceedings -. 153. 750 - 762. 10.1049/ip-epa:20060008.

[55] Remus Teodorescu, Marco Liserre, Pedro Rodríguez (2019). Grid Converters for Photovoltaic and Wind Power Systems. John Wiley & Sons, Ltd. https://doi.org/10.1002/9780470667057.ch10

[56] Lim J-U, Kim H-W, Cho K-Y, Bae J-H. Stand-Alone Microgrid Inverter Controller Design for Nonlinear, Unbalanced Load with Output Transformer. Electronics. 2018; 7(4):55. https://doi.org/10.3390/electronics7040055

[57] Hong-Seok Song and Kwanghee Nam, 'Dual Current Control Scheme for PWM Converter under Unbalanced Input Voltage Conditions'. IEEE Transactions on Industrial Electronics, 46(5), October 1999, 953–959,

[58] A. Tarraso, L. Marín, N. B. Lai and P. Rodriguez, "Enhanced Proportional-Resonant (PR) Controller with Negative Decoupling for Weak Grids," 2020 IEEE 21st Workshop on Control and Modeling for Power Electronics (COMPEL), 2020, pp. 1-4, doi: 10.1109/COMPEL49091.2020.9265663.

[59] Remus Teodorescu, Marco Liserre, Pedro Rodríguez (2019). Grid Converters for Photovoltaic and Wind Power Systems. John Wiley & Sons, Ltd. https://doi.org/10.1002/9780470667057.ch8

[60] Remus Teodorescu, Marco Liserre, Pedro Rodríguez (2019). Grid Converters for Photovoltaic and Wind Power Systems. John Wiley & Sons, Ltd. https://doi.org/10.1002/9780470667057.ch3

[61] Power quality – IEEE 519-2014. Comsys. (2022, April 29). Retrieved August 5, 2022, from https://comsys.se/our-adf-technology/power-qualitieee-519-2014/

[62] S. Elias and A. Rezaei-Zare, "Unified Control Strategy for Microgrid Solid-State Transformers," 2022 IEEE International Conference on Environment and Electrical Engineering and 2022 IEEE Industrial and Commercial Power Systems Europe (EEEIC / I&CPS Europe), 2022, pp. 1-6, doi: 10.1109/EEEIC/ICPSEurope54979.2022.9854558.

[63] Levron, Y., & Belikov, J. (n.d.). Lecture 2: The direct-quadrature-zero (DQ0) transformation - A-lab. www.a-lab.ee. Retrieved August 24, 2022, from https://a-lab.ee/sites/default/files/PS_Lecture_2.pdf

[64] Y. Yonezawa, "Recent Progress in High to Ultra-High-Voltage SiC Power Devices: Development and Application," 2018 International Power Electronics Conference (IPEC-Niigata 2018 -ECCE Asia), 2018, pp. 3603-3606, doi: 10.23919/IPEC.2018.8507668.

[65] B. Hu et al., "A Survey on Recent Advances of Medium Voltage Silicon Carbide Power Devices," 2018 IEEE Energy Conversion Congress and Exposition (ECCE), 2018, pp. 2420-2427, doi: 10.1109/ECCE.2018.8558451.

Appendix (A) – Equations

Inductor current coupling equation 1 $\mathrm{L}\frac{d}{dt}i_d = \omega s\ iq + \frac{v_L}{L}$ (1)

Inductor current coupling equation 2 $\mathrm{L}\frac{d}{dt}i_q = -\ \omega s\ id + \frac{v_L}{L}$ (2)

The abc to dq0 transformation $X_{dq0} = T_\theta \ . \ X_{abc}$ (3)

The abc to dq0 transformation $X_{abc} = {T_\theta}^{-1} \ . \ X_{dq0}$ (4)

$$T_\theta = \frac{2}{3}\begin{bmatrix} \cos(\theta) & \cos\left(\theta - \frac{2\pi}{3}\right) & \cos\left(\theta + \frac{2\pi}{3}\right) \\ -\sin(\theta) & -\sin\left(\theta - \frac{2\pi}{3}\right) & -\sin\left(\theta + \frac{2\pi}{3}\right) \\ \frac{1}{2} & \frac{1}{2} & \frac{1}{2} \end{bmatrix} \quad (5)$$

$${T_\theta}^{-1} = \begin{bmatrix} \cos(\theta) & -\sin(\theta) & 1 \\ \sin\left(\theta - \frac{2\pi}{3}\right) & -\sin\left(\theta - \frac{2\pi}{3}\right) & 1 \\ \cos\left(\theta + \frac{2\pi}{3}\right) & -\sin\left(\theta + \frac{2\pi}{3}\right) & 1 \end{bmatrix} \quad (6)$$

L-filter inductance $\mathrm{L} = \frac{UV_L}{\omega \frac{p}{3}}$ (7)

d-q reference frames coupling equations (8) through (13):

$$Vdq^n = \begin{bmatrix} Vd^n \\ Vq^n \end{bmatrix} = \begin{bmatrix} \bar{V}d^n \\ \bar{V}q^n \end{bmatrix} + \begin{bmatrix} \tilde{V}d^n \\ \tilde{V}d^n \end{bmatrix} \quad (8)$$

$$\begin{bmatrix} \bar{V}d^n \\ \bar{V}q^n \end{bmatrix} = V^n \begin{bmatrix} \cos(\varphi^n) \\ \sin(\varphi^n) \end{bmatrix} \quad (9)$$

$$\begin{bmatrix} \tilde{V}d^n \\ \tilde{V}q^n \end{bmatrix} = V^m \cos(\varphi^m) \begin{bmatrix} \cos((n-m)\omega t) \\ -\sin((n-m)\omega t) \end{bmatrix} + V^m \sin(\varphi^m) \begin{bmatrix} \sin((n-m)\omega t) \\ \cos((n-m)\omega t) \end{bmatrix} \quad (10)$$

$$Vdq^m = \begin{bmatrix} Vd^m \\ Vq^m \end{bmatrix} = \begin{bmatrix} \bar{V}d^m \\ \bar{V}q^m \end{bmatrix} + \begin{bmatrix} \tilde{V}d^m \\ \tilde{V}d^m \end{bmatrix} \quad (11)$$

$$\begin{bmatrix} \tilde{V}d^m \\ \tilde{V}d^m \end{bmatrix} = V^m \begin{bmatrix} \cos(\varphi^m) \\ \sin(\varphi^m) \end{bmatrix} \quad (12)$$

$$\begin{bmatrix}\tilde{V}d^m\\ \tilde{V}q^m\end{bmatrix} = V^n\cos(\varphi^n)\begin{bmatrix}\cos((n-m)\omega t)\\ \sin((n-m)\omega t)\end{bmatrix} + V^m\sin(\varphi^n)\begin{bmatrix}-\sin((n-m)\omega t)\\ \cos((n-m)\omega t)\end{bmatrix} \quad (13)$$

The R-filter transfer function: $\frac{\mathrm{kr}}{s^2+\omega_2^2}$ (14)

The transfer function of the PI controller: $\frac{\mathrm{kp.s+\ ki}}{s}$ (15)

The transfer function of the voltage controller with the R-filter: $\frac{\mathrm{kp.s+\ ki}}{s} + \frac{\mathrm{kr}}{s^2+\omega_2^2}$ (16)